Horizontal and vertical velocities derived from the IDS contribution to ITRF2014, and comparisons with geophysical models

Guilhem Moreaux, Franck G Lemoine, Donald F. Argus, Alvaro Santamaria-Gomez, Pascal Willis, Laurent Soudarin, Médéric Gravelle, Pascale Ferrage

Geophysical Journal International

Geophys. J. Int. (2016) **207,** 209–227
Advance Access publication 2016 July 19
GJI Geodynamics and tectonics

doi: 10.1093/gji/ggw265

Horizontal and vertical velocities derived from the IDS contribution to ITRF2014, and comparisons with geophysical models

G. Moreaux,[1] F.G. Lemoine,[2] D.F. Argus,[3] A. Santamaría-Gómez,[4,5] P. Willis,[6,7] L. Soudarin,[1] M. Gravelle[4] and P. Ferrage[8]

[1] *Collecte Localisation Satellites,* 8-10 *rue Hermès, Parc Technologique du Canal, F-*31520 *Ramonville Saint-Agne, France. E-mail: gmoreaux@cls.fr*
[2] *NASA, Goddard Space Flight Center, Code* 698*, Greenbelt, MD* 20771*, USA*
[3] *Jet Propulsion Laboratory, California Institute of Technology, Pasadena, CA* 91109*, USA*
[4] *LIENSS, Université de La Rochelle-CNRS,* 2 *rue Olympe de Gouge, La Rochelle, France*
[5] *School of Land and Food, University of Tasmania, Hobart, Australia*
[6] *Institut National de l'Information Géographique et Forestière, Direction de la Recherche et de l'Enseignement, Marne-la-vallée, France*
[7] *Institut de Physique du Globe de Paris, UMR*7154*, Gravimétrie et géodésie spatiale, Université Paris Diderot, Sorbonne Paris Cité, Paris, France*
[8] *Centre National d'Etudes Spatiales,* 18 *avenue Edouard Belin, F-*31401 *Toulouse Cedex* 9*, France*

Accepted 2016 July 15. Received 2016 July 13; in original form 2016 April 30

SUMMARY

In the context of the 2014 realization of the International Terrestrial Reference Frame, the International DORIS (Doppler Orbitography Radiopositioning Integrated by Satellite) Service (IDS) has delivered to the IERS a set of 1140 weekly SINEX files including station coordinates and Earth orientation parameters, covering the time period from 1993.0 to 2015.0. From this set of weekly SINEX files, the IDS combination centre estimated a cumulative DORIS position and velocity solution to obtain mean horizontal and vertical motion of 160 stations at 71 DORIS sites. The main objective of this study is to validate the velocities of the DORIS sites by comparison with external models or time-series. Horizontal velocities are compared with two recent global plate models (GEODVEL 2010 and NNR-MORVEL56). Prior to the comparisons, DORIS horizontal velocities were corrected for Global Isostatic Adjustment from the ICE-6G (VM5a) model. For more than half of the sites, the DORIS horizontal velocities differ from the global plate models by less than 2–3 mm yr^{-1}. For five of the sites (Arequipa, Dionysos/Gavdos, Manila and Santiago) with horizontal velocity differences with respect to these models larger than 10 mm yr^{-1}, comparisons with GNSS estimates show the veracity of the DORIS motions. Vertical motions from the DORIS cumulative solution are compared with the vertical velocities derived from the latest GPS cumulative solution over the time span 1995.0–2014.0 from the University of La Rochelle solution at 31 co-located DORIS-GPS sites. These two sets of vertical velocities show a correlation coefficient of 0.83. Vertical differences are larger than 2 mm yr^{-1} at 23 percent of the sites. At Thule, the disagreement is explained by fine-tuned DORIS discontinuities in line with the mass variations of outlet glaciers. Furthermore, the time evolution of the vertical time-series from the DORIS station in Thule show similar trends to the GRACE equivalent water height.

Key words: Satellite geodesy; Reference systems; Plate motions.

1 INTRODUCTION

In the frame of the 2014 realization of the International Terrestrial Reference Frame (ITRF), the International DORIS Service (IDS; Willis *et al.* 2016b) delivered to the IERS (International Earth Rotation and Reference Systems Service) 1140 weekly SINEX files including weekly DORIS (Doppler Orbitography Radiopositioning Integrated by Satellite) station positions and daily pole coordinates. Since ITRF2005, DORIS is one of the four fundamental geodetic techniques contributing to the realization of the ITRS (International Terrestrial Reference System). The new IDS series (IDS 09) is the combination of multisatellite weekly SINEX solutions from the six IDS analysis centres over the time span from 1993 January to 2014 December. The number of different DORIS individual solutions coupled with the software packages diversity reduces systematic software-dependent errors and helps to achieve a reliable IDS combination. Compared to the IDS contribution to ITRF2008 (Altamimi *et al.* 2011), the IDS 09 differs on the DORIS satellite constellation,

the DORIS tracking network and the data modeling. Since 2008, the DORIS space segment evolved significantly with the launch of four new satellites (Jason-2, Cryosat-2, HY-2A and Saral) equipped with the latest (third) generation of DORIS receivers. That new type of the DORIS receiver (the so-called DGXX receiver) can track up to seven beacons simultaneously, resulting in a significant increase in the number of available measurements especially at lower elevations. In the same period of time, three DORIS satellites (Envisat, SPOT2 and SPOT4) were decommissioned. Since mid-2009, after the submission of solutions to ITRF2008, the DORIS tracking network also improved, mainly due to the DORIS ground station renovation program. As a result, in addition to being homogeneously geographically distributed, the tracking network is more uniform in terms of beacon and antenna generation model as well as in terms of antenna support type. In addition to these DORIS technical evolutions, the modeling of the DORIS measurements and the satellite modeling also improved. The data processing of the IDS 09 series includes the implementation of beacon frequency offset estimations (i.e. difference between actual frequency and the nominal value) and uses DORIS ground antenna phase centre variations (PCVs; Tourain *et al.* 2016). Due to their low orbital altitudes (700–1340 km), the DORIS satellites are more sensitive to the time-variable geopotential (e.g. EIGEN-6S2; Rudenko *et al.* 2014). Therefore, making benefit of new geopotential models using Gravity Recovery And Climate Experiment (GRACE; Tapley *et al.* 2004) data, the IDS analysis centres adopted geopotential models that included more detailed time-variable gravity modeling. For the realization of the ITRF2008, as the Jason-1 ultrastable oscillator (USO) was known to exhibit high sensitivity to passage through the South Atlantic Anomaly (SAA), that mission was not included in the DORIS mission list. Taking advantage of the development of a Jason-1 SAA-correction model by Lemoine & Capdeville (2006), while processing their contribution to ITRF2014 (Altamimi *et al.* 2016), the IDS analysis centres were encouraged to use the Jason-1 SAA-corrected data. In addition, since the delivery of the IDS contribution to ITRF2008, Štěpánek *et al.* (2014) have pointed out the USO on SPOT5 also experiences perturbations after passage through the SAA. Similarly to Jason-1, Capdeville and Lemoine developed a SAA data correction model for SPOT5 (Capdeville *et al.* 2016). Then, all the ACs were asked to use the SPOT5 SAA-corrected data starting on SPOT5 cycle 138 (2005 December 27). As a consequence, the IDS contribution to ITRF2014 exhibits more accurate translation and scale parameters and vertical positioning performances are improved. For more details on the combination process, impact on the new modeling standards and evaluation in terms of transformation parameters, Earth orientation parameters and station position performance of the IDS 09 series, see Moreaux *et al.* (2016).

As part of the validation process of the IDS contribution to ITRF2014, the IDS combination centre (CC) determined a cumulative DORIS position and velocity solution from the 1140 SINEX files which have been delivered to IERS. The first aim of that cumulative solution was to better estimate the positioning performances of the new IDS combined solution. As IDS 09 standards introduced notable differences to the IDS contribution to ITRF2008 in vertical positioning, we thought it more reliable to evaluate its positioning performances with an internal cumulative solution rather than with ITRF2008. The second objective of the IDS 09 cumulative position was for the IDS CC to be in position to succeed to Willis in the routine processing of a DORIS-oriented terrestrial reference frame for Precise Orbit Determination (Willis *et al.* 2009,2016a). That so-called DPOD is an extension of the current ITRF solution to reflect the complete set of available DORIS stations. The third objective of the IDS 09 cumulative position was to further analyse possible interests of DORIS in studying local Earth motion (e.g. small tectonic plates) and/or global kinematic. Indeed, owing to its global and homogeneous tracking network, the DORIS technique can contribute to the elaboration of global plate motions (Crétaux *et al.* 1998; Soudarin & Crétaux 2006; Argus *et al.* 2010; Kreemer *et al.* 2014). DORIS can also provide motion estimates for plates where the geodetic network is rather sparse such as Africa (Nocquet *et al.* 2006; Saria *et al.* 2013) or Antarctica (King & Santamaría-Gómez 2016). Moreover, the location of some of the DORIS stations at plate boundary zones can help to better understand local tectonic phenomena (Bettinelli *et al.* 2006). In addition, vertical motions derived from DORIS can be used to either determine or validate Glacial Isostatic Adjustment (GIA) models (King *et al.* 2010; Argus *et al.* 2014; Peltier *et al.* 2015).

In this paper, we present the validation of both the horizontal and vertical motions deduced from the IDS cumulative solution. We first compute the cumulative position and velocity solution from the 1140 files of the IDS 09 series (Section 2). Then, we correct the observed horizontal velocities for GIA contribution (Section 3). In Section 4, we compare the obtained horizontal velocities of the DORIS sites with those expected from two recent global plate models: NNR-MORVEL56 (Argus *et al.* 2011) and GEODVEL (Argus *et al.* 2010), and we discuss five sites (Arequipa, Dionysos/Gavdos, Manila and Santiago) with velocities differing significantly from at least one of the two plate models by comparing with observations from relevant GPS stations. Section 5 deals with the validation of the vertical velocities from the DORIS cumulative solution with respect to vertical motions derived from the GPS ULR solution, updated from Santamaría-Gómez *et al.* (2012). Sites which show larger differences in vertical velocities (Thule and Ny-Ålesund) are of special concern. Finally, we provide new perspectives and discuss future challenges for the IDS CC (Section 6).

2 IDS CUMULATIVE SOLUTION

To estimate the DORIS station velocities, time-series of the 160 stations from the 1140 IDS 09 weekly SINEX files were accumulated into a long-term frame solution using the CATREF (Combination and Analysis of Terrestrial Reference Frames) package (Altamimi *et al.* 2002) from IGN (Institut National de l'information Géographique et forestière). To ensure a more reliable velocity determination and to minimize the impact of seasonal signals on the velocities, the sites with less than 2.5 yr of observations were not included in the IDS 09 series. Each weekly terrestrial frame was aligned onto the long-term frame by estimating the seven Helmert (translations, rotations and scale) transformation parameters. To overcome rank deficiency of the normal equation system while computing the long-term frame and to apply the No-Net-Rotation (NNR) condition, minimal constraints on origin, scale and orientation were added to align the long-term frame on ITRF2008. This alignment was realized with respect to the reference positions and velocities of a core network. The core network was initialized with the stations belonging to the DORIS sites with more than 500 weeks of observations over the 1140 weeks of the entire data span. Then, the core network was fine-tuned to improve the homogeneous global distribution (see Fig. 2) with 19 (respectively 18) sites in the northern (respectively southern) hemisphere. Priority was given to the stations with longer time-series. Station position discontinuities were introduced by visual inspection of the station position time-series displayed from the IDS Web Service (http://ids-doris.org/webservice/).

History of earthquakes and equipment (e.g. USO and antenna) upgrades at all the DORIS sites is of great help for the elaboration of a preliminary set of discontinuities. Then, station position discontinuities were refined while computing the cumulative solution by looking at the station position residuals (differences between the weekly estimate and the linear model). After several iterations, we ended up with 62 discontinuities (see Table 1): 26 of them have a seismic origin, 9 can be linked to a beacon or antenna technical events (e.g. USO failure), 2 are due the velocity change in Thule and 25 have so far no explanation. Furthermore, these 62 discontinuities concern 32 of the 71 DORIS sites (see Fig. 1). Thus, the IDS cumulative solution contains coordinates of $160 + 62 = 222$ stations at 71 sites. The normal equation system of the cumulative solution was also constrained by the use of the DORIS–DORIS local ties (3-D vector between two successive station installations at the same DORIS site) from IGN. We count in total 100 tie vectors. Note that the uncertainties of the tie vectors were revisited after analysis of the coordinate differences at the end of the first iteration of the cumulative process. In addition, no tie vector was used to connect stations which experienced a seismic event. Moreover, we tightly constrained velocities to the same value over multiple segments unless a velocity discontinuity was observed (e.g. due to an earthquake). Such velocity constraints make short periods of data before or after a position discontinuity to benefit from the estimated velocity of longer periods at the same site. Five cumulative DORIS solutions were iteratively processed to remove absolute and relative (ratio of position difference by position error) position outliers while approximating station displacements by a linear model. Comparison of the estimated tie vectors with the IGN ones showed discrepancies larger than 4 cm for at least one component for four of them (see Fig. 3): AREB-ARFB (Arequipa), ASDB-ASEB (Ascension), MARB-MATB (Marion Island) and TRIA-TRJB (Tristan Da Cunha). The tie vector residuals correspond to the differences between the estimated and reference (from IGN) tie vectors. The estimated tie vectors are set to the difference of the station coordinates at the first epoch of the newest station as no date of the reference tie vectors was given. The discrepancy in Arequipa and Tristan Da Cunha may result from a period of time with no beacon longer than 3 yr as well as from the estimation procedure of the residuals. In Marion Island, the difference in the tie vectors may be the consequence of the South Africa earthquake of magnitude 5.4 which happened in 2002 June 16. Hereafter, we only retain velocities with formal error less than 1 mm yr^{-1} in either horizontal (Figs 4 and 6) or vertical plane (Figs 5 and 7). Over the 222 stations at 71 sites, 191 (respectively 201) horizontal (respectively vertical) velocities at 67 (respectively 70) sites are associated with uncertainties lower than 1 mm yr^{-1}. The rejected sites are: Arlit (1.34 mm yr^{-1}), Grasse (1.12 mm yr^{-1}), Monument Peak (1.38 mm yr^{-1}) and Canberra (1.93 mm yr^{-1}) with respect to the horizontal velocity and Canberra (1.22 mm yr^{-1}) due to the formal error of the vertical motion. The slightly higher velocity formal errors of these sites are the consequence of shorter observation time spans as Arlit, Canberra, Grasse and Monument Peak are among the top seven of the DORIS sites with the fewest number of weeks in the combined solution files (see fig. 7 from Moreaux *et al.* 2016).

3 GLOBAL ISOSTATIC ADJUSTMENT

The DORIS motion contains contributions from the elastic deformation of the Earth to ongoing mass changes (including ice changes) as well as from the viscoelastic response due to past glacial changes (i.e. GIA). GIA, also called PGR which stands for Postglacial Rebound, is the response of the Earth to the mass redistributions associated with the glacial cycles in the Late Pleistocene. At present, GIA is observed at former- and present-day glaciated regions. In areas that are currently glaciated such as Greenland and Antarctica, the GIA response is mixed with the present-day response caused by the ongoing melting. At former glaciated regions such as Fennoscandia and North America, crustal displacement related to GIA can be measured directly by GPS or DORIS receivers.

Whereas the linear velocities resulting from the IDS combination are affected by GIA, the horizontal velocities as output of the plate models are free of GIA. Therefore, that geophysical effect must be subtracted from the DORIS velocities (for the DORIS sites in areas where GIA occurs) before any comparison with the plate models. We selected one of the most recently developed global GIA models: the ICE-6G (VM5a) model from Peltier *et al.* (2015). That model combines observations of relative sea level over the past 20 kyr with GPS data. Horizontal and vertical motions at 69 of the 71 DORIS sites were extracted from north, east and up GIA velocities at the geodetic sites (ASCII file GS_vels.txt) from Peltier's web site (http://www.atmosp.physics.utoronto.ca/~peltier/). Over the 71 DORIS sites, from ICE-6G we extracted GIA velocities at 58 DORIS sites and deduced it at 11 more sites due to co-locations with either GPS or tide gauge stations (see Fig. 8). The two DORIS sites with no GIA modelization are Gavdos and Crozet.

4 EVALUATION OF THE DORIS HORIZONTAL VELOCITIES

This section aims at evaluating the horizontal velocities from the IDS 09 cumulative solution at the DORIS sites. Thus, we compare the DORIS velocities to two recent geodetical (GEODVEL) and geological (NNR-MORVEL56) plate models. After a brief description of the two global plate models we used for the validation of our horizontal velocities, we discuss sites where the DORIS horizontal velocities differ significantly from the global model estimates and, if available, we compare the DORIS estimates to either GNSS or VLBI solutions as extracted at co-located sites.

4.1 Global plate models

GEODVEL (for GEODesy VELocity; Argus *et al.* 2010) is a plate model obtained by combination of solutions from the four space geodetic techniques: DORIS, GNSS, SLR and VLBI. Each technique solution was determined by one analysis institution. Estimations of angular velocities of 11 major plates (Antarctica, Arabia, Australia, Eurasia, India, Nazca, North America, Nubia, Pacific, Somalia and South America) are based on nearly 31 yr of observations (from 1976 to 2007). Only sites located in places associated to the rigid category (places on plate interiors with insignificant GIA) were retained for the angular velocity estimations. As a consequence, sites affected by GIA were not used. In the case of DORIS, the contribution to GEODVEL was provided by Pascal Willis from the IGN IDS analysis centre. Velocities at 60 DORIS sites were estimated from weekly positions between 1993 January and 2006 January. In addition to the data span, the IGN contribution to GEODVEL differs from the IGN contribution to IDS 09 mainly by use of both time-variable gravity field and DORIS ground antenna PCVs. Estimations of horizontal velocities from the GEODVEL model at DORIS sites were

Table 1. IDS 09 discontinuities as determined by the IDS CC.

Beacon Acronym	Site	DOMES Number	Discontinuity Date (Year:Doy:Sec)	Origin of discontinuity
ADEA	Terre Adélie	91501S001	1998:084:00000	Earthquake 1998 March 25 (8.1)
ADGB	Terre Adélie	91501S004	2014:161:00000	Beacon change
AMTB	Amsterdam Isand	91401S003	2005:327:00000	Antenna offset (2005 November 24)
ARFB	Arequipa	42202S007	2008:190:33187	Earthquake 2008 July 08 (6.2)
ARFB	Arequipa	42202S007	2010:126:09767	Tarapaca Earthquake 2010 May 06 (6.2)
ARFB	Arequipa	42202S007	2012:159:57780	Earthquake 2012 June 07 (6.1)
ASDB	Ascension	30602S004	2007:174:00000	Unknown 2007 June 23
CADB	Cachoeira	41609S002	2008:183:00000	Beacon change
CADB	Cachoeira	41609S002	2011:355:00000	Unknown 2011 December 21
CHAB	Chatham Island	50207S001	2006:340:00000	Antenna problem (2006 December XX)
CIDB	Cibinong	23101S003	2009:245:28500	Java Earthquake 2009 September 02 (7.0)
COLA	Colombo	23501S001	1994:320:00000	Earthquake 1994 November 16
EASB	Easter Island	41703S009	2011:186:00000	Beacon change
EASB	Easter Island	41703S009	2012:340:00000	Unknown 2012 December 05
EVEB	Everest	21501S001	2002:075:00000	Frequency offset
EVEB	Everest	21501S001	2011:261:45600	Sikkim Earthquake 2011 September 18 (6.9)
FAIB	Fairbanks	40408S005	2002:307:79961	Central Alaska Earthquake 2002 November 03 (7.9)
FAIB	Fairbanks	40408S005	2003:033:00000	Post seismic
FAIB	Fairbanks	40408S005	2003:215:00000	Post seismic
FAIB	Fairbanks	40408S005	2006:001:00000	Post seismic
GOMB	Goldstone	40405S037	1999:289:35204	Hector Mine Earthquake 1999 October 16 (7.1)
HELB	Saint-Helena	30606S003	2000:035:00000	Antenna tilt
HEMB	Saint-Helena	30606S004	2008:209:76542	Earthquake 2008 July 27 (5.9)
HEMB	Saint-Helena	30606S004	2011:355:00000	Beacon change
KESB	Kerguelen	91201S004	2004:036:00000	Unknown 2004 February 05
KIUB	Kitab	12334S006	2013:146:22080	Uzbekistan Earthquake 2013 May 26 (5.7)
KRAB	Krasnoyarsk	12349S001	1998:246:00000	Unknown 1998 September 03
KRUB	Kourou	97301S004	1997:001:00000	Unknown 1997 January 01
KRUB	Kourou	97301S004	2005:117:00000	Unknown 2005 April 27
KRUB	Kourou	97301S004	2008:037:00000	Unknown 2008 February 06
LICB	Libreville	32809S004	2008:215:00000	Unknown 2008 August 02
MAHB	Mahé	39801S005	2009:089:00000	Beacon change
MANB	Manila	22006S002	2004:192:00000	Frequency offset
MANB	Manila	22006S002	2010:027:67740	Philippine Earthquake 2010 January 27 (5.9)
MANB	Manila	22006S002	2012:168:80280	Luzon Earthquake 2012 June 16 (5.9)
MARB	Marion Island	30313S002	2002:167:64760	Earthquake 2002 June 16 (5.4)
PDMB	Ponta Delgada	31906S002	2008:160:00000	USO change
REYB	Reykjavik	10202S002	2000:169:56460	Iceland Earthquake 2000 June 17 (6.5)
REZB	Reykjavik	10202S003	2005:073:00000	Unknown East and North 2005 March 14
RIOB	Rio Grande	41507S004	1998:080:00000	Unknown in North and Up 1998 March 21
ROTA	Rothera	66007S001	2002:013:00000	Frequency offset
SAKA	Yuzhno-Sakhalinsk	12329S001	1994:282:28539	Kuril Islands Earthquake 1994 October 09 (7.3)
SAKA	Yuzhno-Sakhalinsk	12329S001	1998:360:00000	Unknown 1998 December 26
SAKA	Yuzhno-Sakhalinsk	12329S001	2003:268:71406	Hokkaido Earthquake 2003 September 25 (7.4)
SANB	Santiago	41705S009	2003:147:30585	San Juan Earthquake 2003 May 27 (5.7)
SANB	Santiago	41705S009	2008:256:00000	Unknown 2008 September 12
SANB	Santiago	41705S009	2010:058:23654	Chile Earthquake 2010 February 27 (8.8)
SANB	Santiago	41705S009	2011:045:13200	Maule Earthquake 2011 February 14 (6.7)
SODA	Socorro Island	40503S003	1995:360:00000	Volcanic activity
SODA	Socorro Island	40503S003	1997:149:00000	Volcanic activity
SODB	Socorro Island	40503S004	2002:276:00000	Unknown 2002 October 03
SYPB	Syowa	66006S003	2008:194:00000	Unknown 2008 July 12
SYPB	Syowa	66006S003	2012:193:00000	Unknown 2012 July 11
THUB	Thule	43001S005	2006:150:00000	Vertical motion change
THUB	Thule	43001S005	2013:059:00000	Vertical motion change
TLSB	Toulouse	10003S005	2012:301:00000	Unknown 2012 October 27
TRIA	Tristan Da Cunha	30604S001	1999:198:00000	Unknown 1999 July 17
TRIB	Tristan Da Cunha	30604S002	2004:228:00000	Unknown 2004 August 15
TRIB	Tristan Da Cunha	30604S002	2009:230:00000	Unknown 2009 August 18

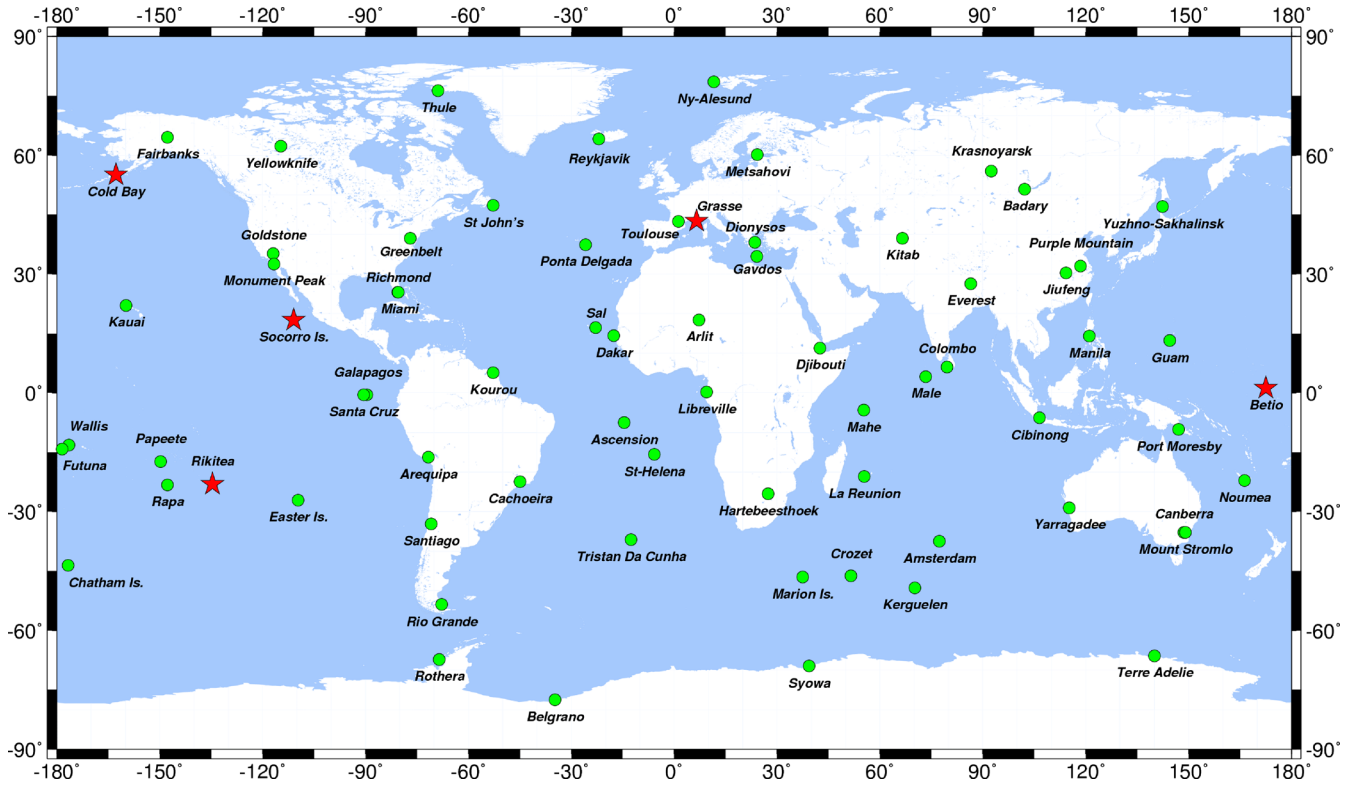

Figure 1. Geographical distribution of the 71 DORIS sites included in the IDS contribution to ITRF2014 (red stars indicate new sites with regard to ITRF2008).

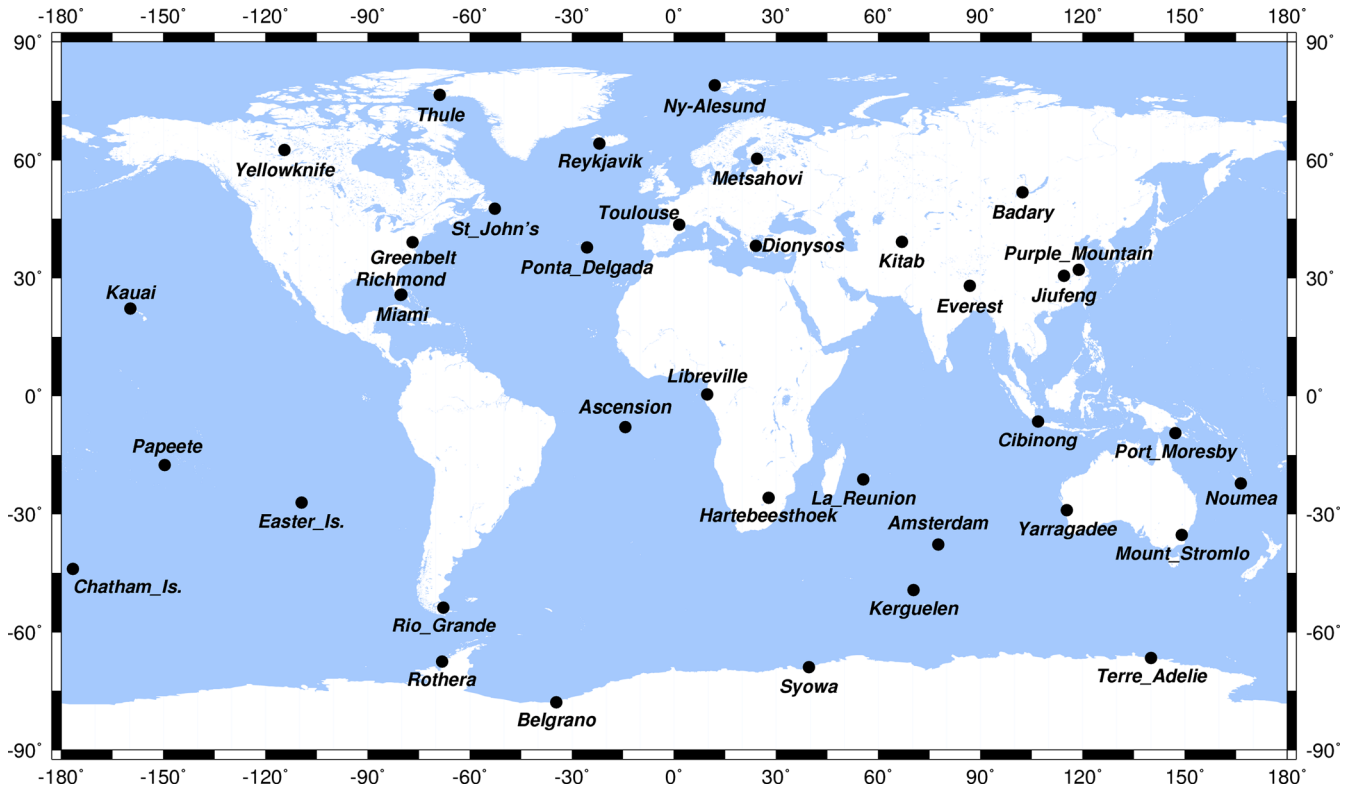

Figure 2. Geographical distribution of the network for NNR condition with respect to ITRF2008.

performed through the UNAVCO plate motion calculator web site (https://www.unavco.org/software/geodetic-utilities/plate-motion-calculator/plate-motion-calculator.html). Fig. 9 illustrates the 66 site velocity differences between GEODVEL and IDS 09 predictions. Inspecting the histogram of the differences (see Fig. 10), we can see that there are differences up to 2 mm yr^{-1} for a majority (around 60 percent) of stations and larger than 7.5 mm yr^{-1} for some others (around 17 percent). The sixteen stations

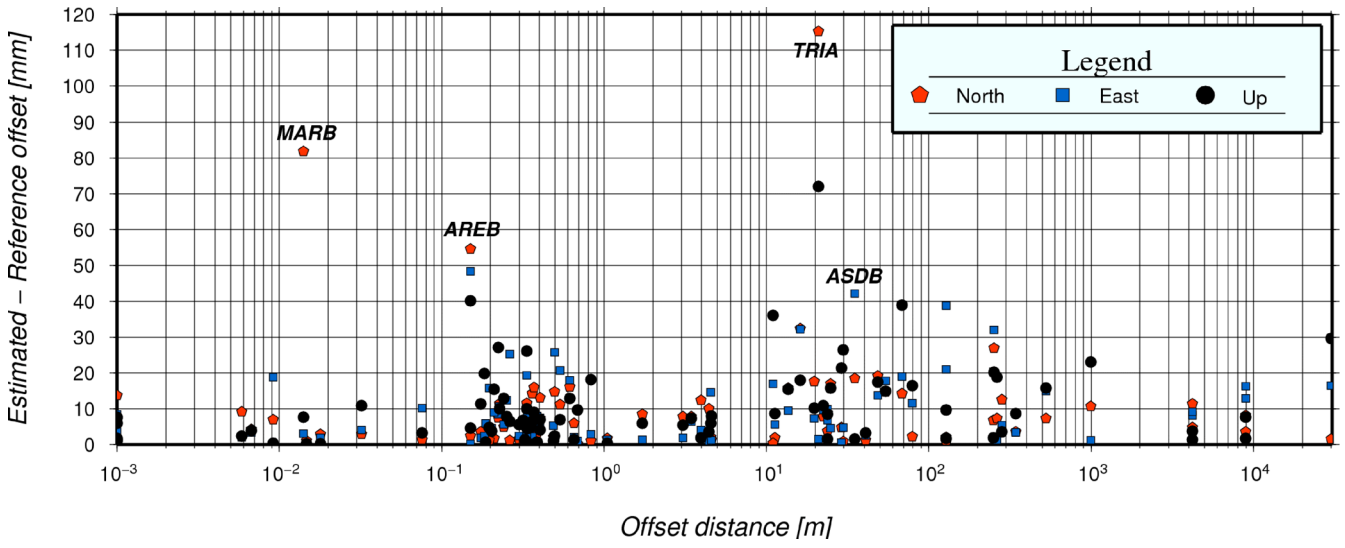

Figure 3. Comparison between residual and reference ties.

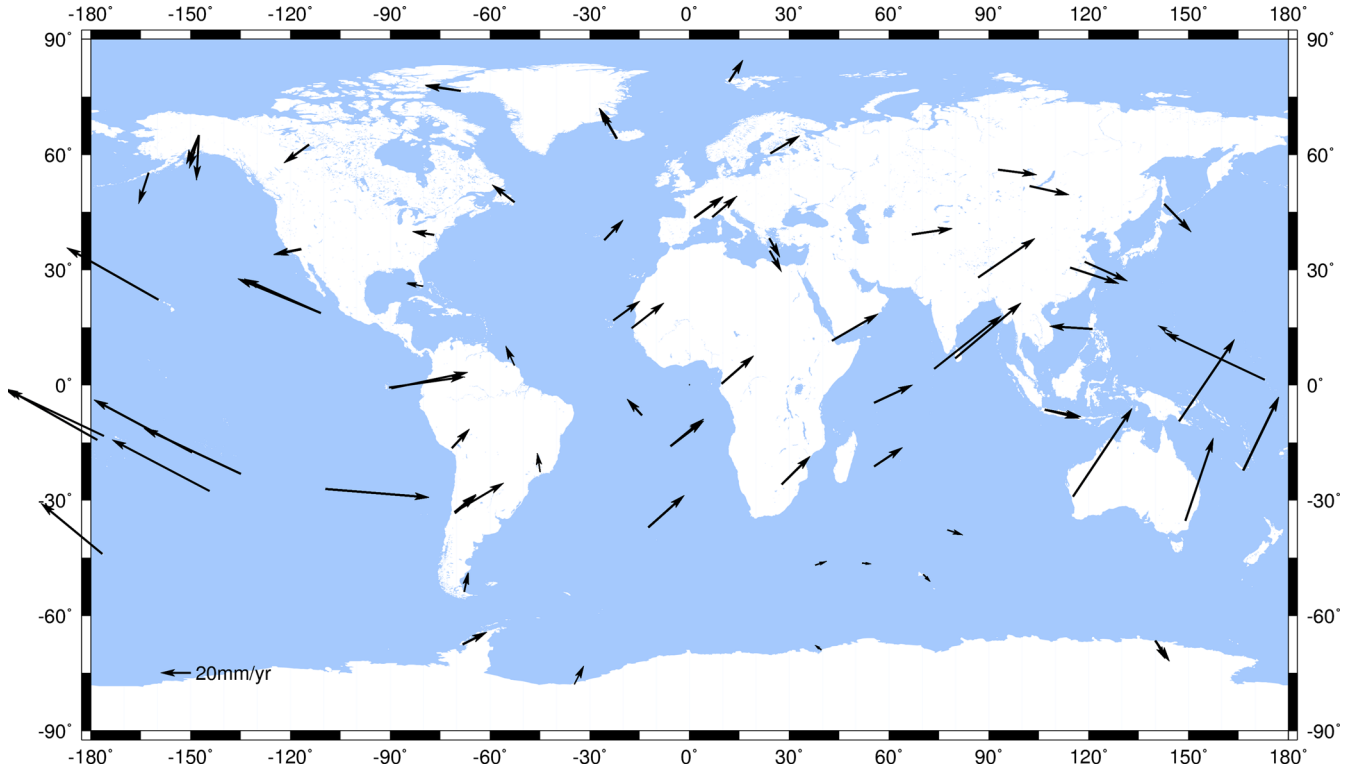

Figure 4. Horizontal velocities at the DORIS sites from the IDS 09 weekly files.

with differences larger than 10 mm yr^{-1} are located at the seven sites (Arequipa, Dionysos, Djibouti, Everest, Gavdos, Manila and Santiago) with black arrows on Fig. 9. The rms of all the differences is 5.5 mm yr^{-1} in the north direction and 8.8 mm yr^{-1} in the east direction. Note that GEODVEL returns no estimation for Guam as it does not include the Philippine Sea plate. If we restrict the differences to the DORIS sites located in the plate interiors (stars on Fig. 9) then, the rms of the differences is 1.8 mm yr^{-1} in the north direction and 2.1 mm yr^{-1} in the east direction.

The NNR-MORVEL56 model (Argus *et al.* 2011) is a complemented version of the geological plate model MORVEL (DeMets *et al.* 2010). Despite its name, which stands for Mid-Ocean Ridge VELocity and is due to the fact that more than three-fourths of the MORVEL data come from the mid-ocean ridges, MORVEL describes the motions of the tectonic plates. The complement consists in the addition of 31 plates from Bird (2003) to the 25 original major plates depicted by Fig. 11. For 20 of the 25 plates that comprise MORVEL, their relative motions are estimated using geological observations (rates of seafloor spreading, directions of oceanic transform faults from swath-mapping sonar and horizontal slip directions during Earthquakes) that average plate motions over 780,000 yr to 3.2 Myr. For six smaller plates (Amur, Caribbean, Philippine Sea, Scotia, Sundaland and Yangtze) with few or no reliable geological data to estimate their motions, GPS

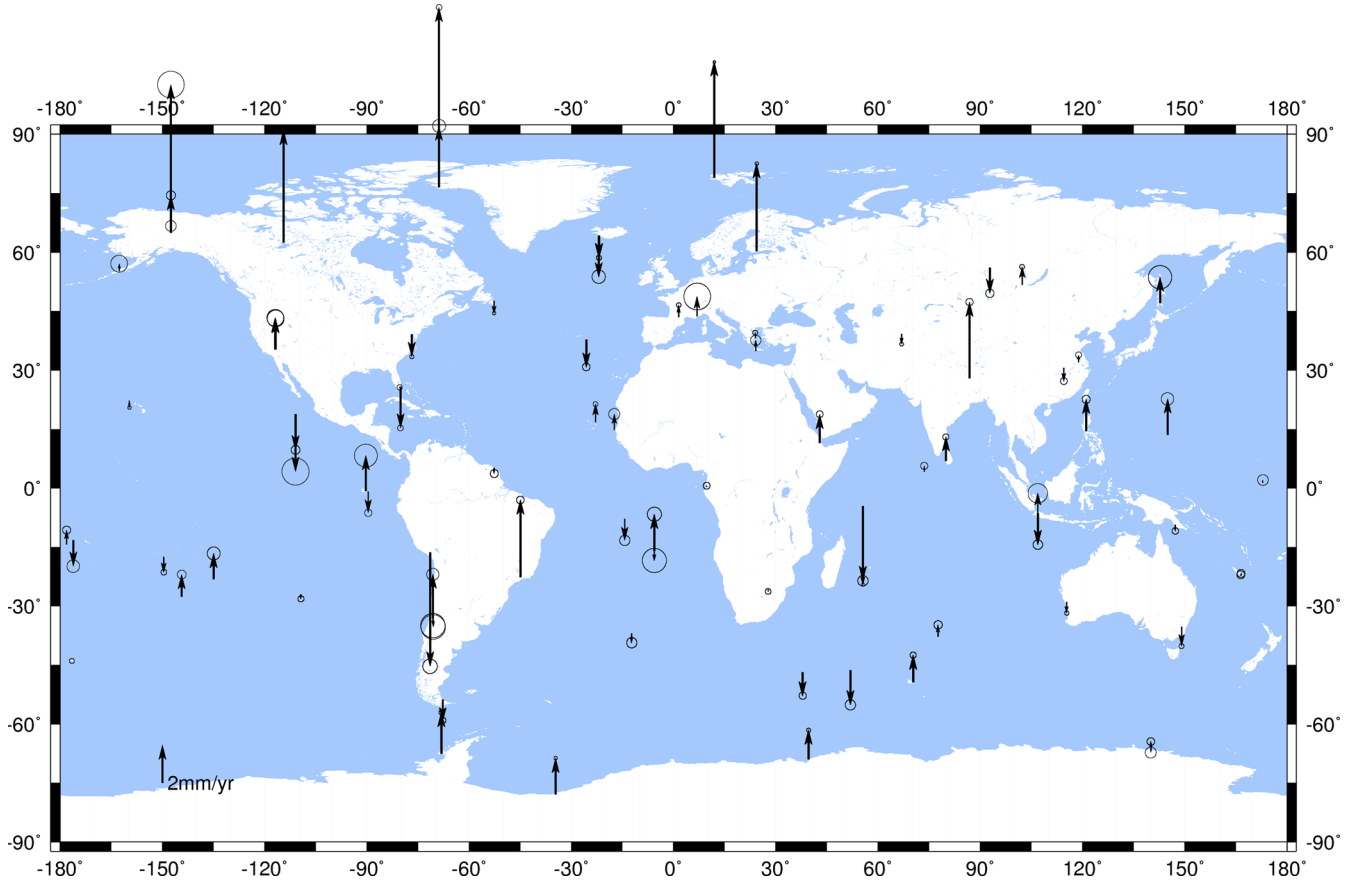

Figure 5. Vertical velocities at the DORIS sites from the IDS 09 weekly SINEX files.

data over 10 yr were used to link their motions to other plates. Estimations of horizontal velocities from the NNR-MORVEL56 model at DORIS sites were performed through the dedicated web site (http://geoscience.wisc.edu/~chuck/MORVEL/motionframe_nnrm56.html). Fig. 11 displays velocity differences between NNR-MORVEL56 and IDS 09 predictions at the 67 DORIS sites with formal errors lower than 1 mm yr^{-1}. From the histogram of the differences (see Fig. 12), we can see that there are differences up to 3 mm yr^{-1} for a majority of stations (nearly 55 percent) and larger than 7.5 mm yr^{-1} for some others (around 5 percent). The 10 stations with differences larger than 10 mm yr^{-1} are located at the five sites (Everest, Goldstone, Guam, Manila and Santiago) with black arrows on Fig. 11. The rms of all the differences is 4.7 mm yr^{-1} for the north component and 9.1 mm yr^{-1} for the east component. If we restrict the differences to the DORIS sites located in the plate interiors (stars on Fig. 11), then the rms of the differences is 2.2 mm yr^{-1} in the north direction and 2.3 mm yr^{-1} in the east direction. As observable with GEODVEL, the major improvement is for the east direction.

4.2 Discussion on horizontal velocity estimates

As depicted by Figs 9 and 11, after removal of the GIA effect on the DORIS velocities, horizontal motions from the IDS 09 cumulative solution agree well with estimations from GEODVEL and NNR-MORVEL56 plate models for most of the DORIS sites. We also observed that the differences are higher in east than in the north direction. This can be fully explained by the conjunction of two features of the DORIS technique: (i) the Doppler technique provides observations that lack information in the direction perpendicular to the satellite track and, (ii) except for TOPEX/Poseidon, Jason-1 and Jason-2, all the DORIS satellites have a near-polar orbit. As expected since plate models do not use observations close to plate boundaries while estimating the angular velocity of the plates, the larger differences (red dots and black arrows in Figs 11 and 9) between the DORIS estimates and the two plate models occur in majority close to the plate boundaries. These differences may also reflect the fact that, whereas the DORIS estimations reveal current motions, the plate models account for deformation over older (and longer) time periods. Meanwhile, as the first concern of this paper is the validation of the DORIS velocities, and as the DORIS estimations may be useful for further local studies on the ongoing phenomena, hereafter we discuss on the validity of the DORIS horizontal velocities for the five sites (Arequipa, Dionysos/Gavdos, Manila and Santiago) which present the largest discrepancies with the two plate models. For the Everest and Goldstone sites where the IDS velocities differ between the two plate models by more than 10 mm yr^{-1}, comparisons with the GPS coordinate time-series from the Nevada geodetic laboratory (http://geodesy.unr.edu/index.php) show differences smaller than 1.5 mm yr^{-1}. In Djibouti, the IDS, GEODVEL and NNR-MORVEL horizontal velocity vector present similar directions and only differ in amplitude.

4.2.1 Arequipa (Peru)

Fig. 13 displays horizontal velocity of Arequipa (Peru) from the IDS cumulative solution, two models GEODVEL and NNR-MORVEL56 as well as from the IGS and ILRS stations as

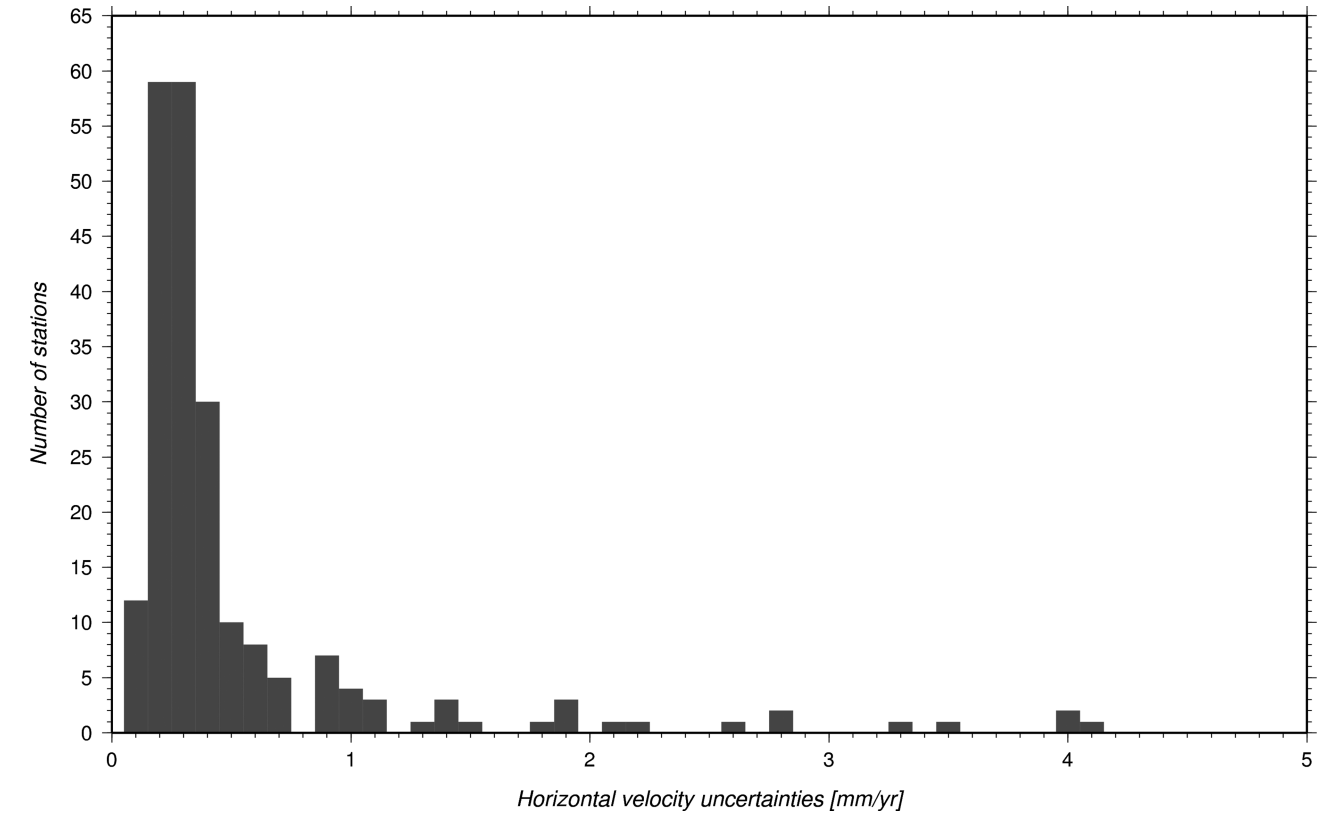

Figure 6. Histogram of the horizontal velocities uncertainties at the DORIS sites from the IDS 09 weekly SINEX files.

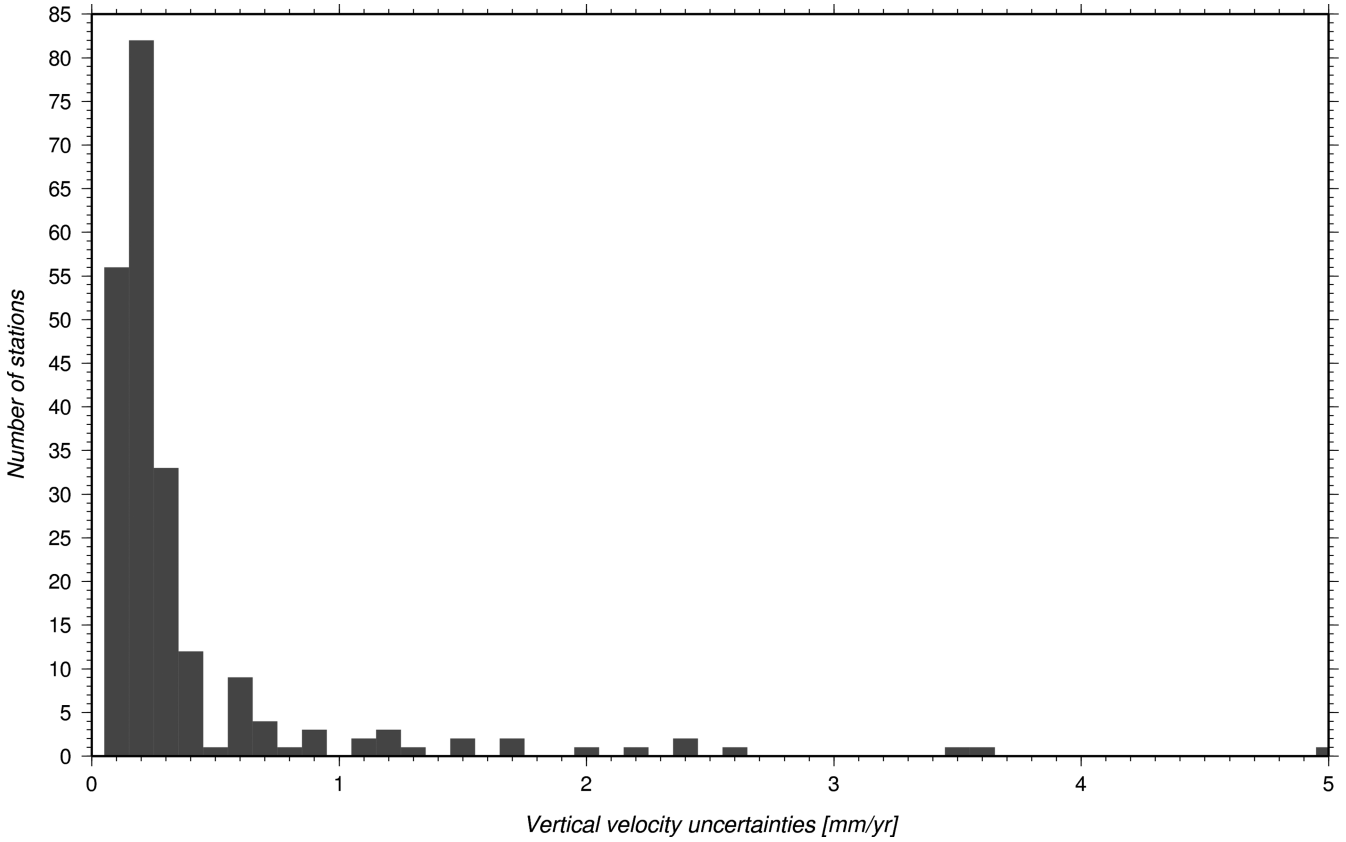

Figure 7. Histogram of the vertical velocities uncertainties at the DORIS sites from the IDS 09 weekly SINEX files.

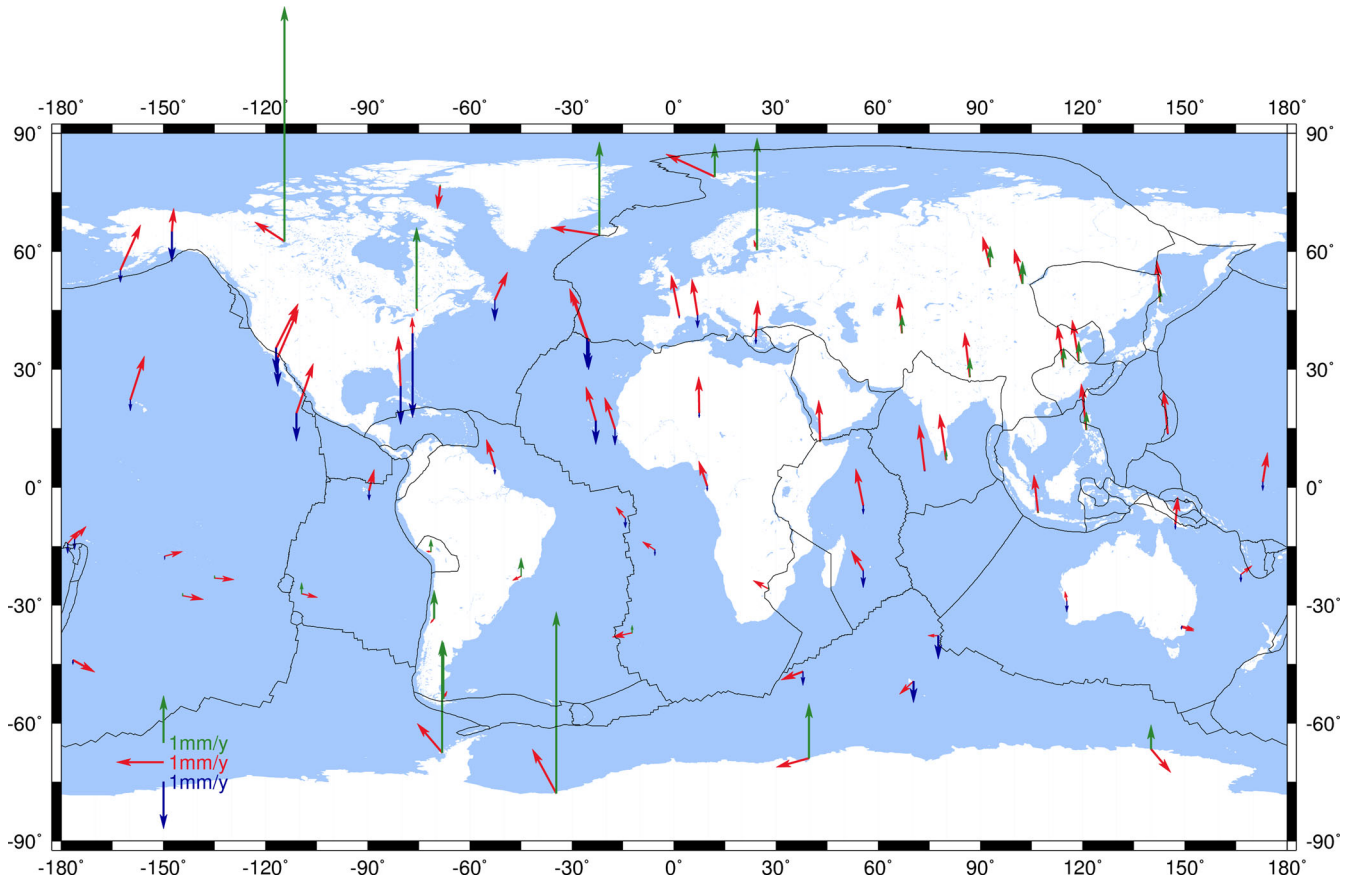

Figure 8. GIA velocities at the DORIS sites from ICE-6G. Horizontal motion is depicted by red arrows while uplift (respectively subsidence) is displayed by green (respectively blue) arrows.

extracted from ITRF2008 (Altamimi *et al.* 2011). The IGS (respectively ILRS) station AREQ (respectively marker 7907) is located at 36 m (respectively 13 m) from the DORIS AREB station. The very short distances between the geodetic stations make relevant the comparisons of the intratechnique estimations. From Fig. 13, we observe that the GEODVEL vector has a different orientation compared to the others. That pattern may reflect the fact that the GEODVEL model associates Arequipa to the major South America (SA) plate while the NNR-MORVEL56 model integrates the small Altiplano (AP) plate and, thus may better model the local displacement of that deformation zone. As Arequipa is located close to plate boundaries, the DORIS, GPS and Laser observations for that site have not been used in GEODVEL processing to compute the South America plate motion. Then, if instead of estimating the GEODVEL motion of Arequipa from the plate angular velocity we go back to the GEODVEL input data (table 4c of Argus *et al.* 2010)—grey arrow in Fig. 13, the new GEODVEL horizontal displacement gives better agreement with the ones. The computation of the relative displacement of Arequipa with respect to the South America plate from IDS 09 estimations and GEODVEL plate prediction shows an eastward motion.

4.2.2 Dionysos and Gavdos (Greece)

We observe discrepancies between DORIS estimates and the two plate models in Greece. IDS 09 velocities have been obtained from observations between late 2003 (respectively early 1994) and early 2012 (respectively late 2014) for Gavdos (respectively Dionysos) and that no position or velocity discontinuity has been introduced. Horizontal speed vectors of Dionysos and Gavdos (an island 40 km south of Crete—see Fig. 14) from IDS 09 agree well in both amplitude and azimuth with NNR-MORVEL56 predictions but are nearly orthogonal to the GEODVEL vectors. From that figure, we also see that the new GAVDOS DORIS horizontal motion is consistent with both DORIS and GPS (GVDO station located 17 m from GAVB) estimations from Willis *et al.* (2013) over a shorter time span. The disagreement between GEODVEL and the others must be explained by the fact that NNR-MORVEL56 makes use of a local small plate (Aegean Sea—AS) with motion from McClusky *et al.* (2010) whereas for GEODVEL these two sites belong to the Eurasia (EU) plate. According to IDS 09 and GEODVEL, the relative motion of both Gavdos and Dionysos is in line with southwestward motion of the Aegean region with respect to Eurasia at 30 mm yr^{-1}. Moreover, the similarity in both magnitude and orientation of the DORIS velocities for Gavdos and Dionysos supports the observation from McClusky *et al.* (2010) that Dionysos appears to be moving along with the southern Aegean and so that these two sites belong to the same small plate: the SW Aegean/Pelopponnisos plate (McClusky *et al.* 2010, Fig. 9).

4.2.3 Manila (Philippines)

For the site of Manila (Philippines), the IDS 09 vector is nearly in the opposite direction of the horizontal vectors from the two plate models (see Fig. 15). Even if according to the two models Manila does not belong to the same tectonic plate (Sundaland for

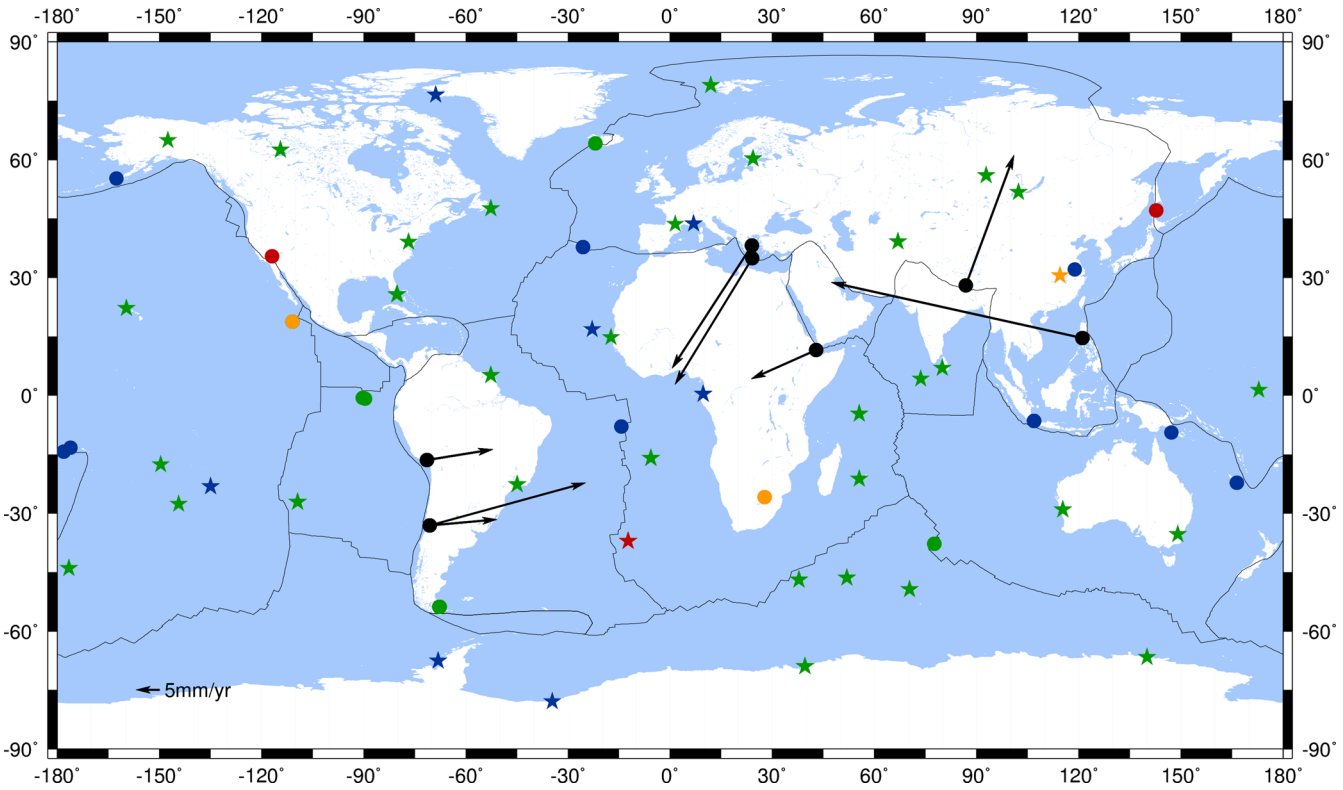

Figure 9. Horizontal velocity differences between IDS 09 and GEODVEL (velocities of the latter are subtracted from the former). Green: less than 2.5 mm yr^{-1}. Blue: between 2.5 and 5.0 mm yr^{-1}. Orange: between 5.0 and 7.5 mm yr^{-1}. Red: between 7.5 and 10.0 mm yr^{-1}. Black: larger than 10 mm yr^{-1}, and rates of velocity differences are shown only in this case. Grey lines indicate plate boundaries used in the NUVEL-1A model and stars denote sites in plate interiors.

NNR-MORVEL56 and Eurasia for GEODVEL), the two vectors give similar directions. Such discrepancies between DORIS solutions and tectonic models in Manila were already shown by Soudarin & Crétaux (2006) while comparing one single DORIS solution to the PB2002 plate model (Bird 2003). According to Bird (2003), Manila is located on the so-called Philippines orogen. An orogen is defined as a small zone of unmodeled complexity. Therefore, differences between the observed (IDS) and predicted (NNR-MORVEL56 and GEODVEL) horizontal velocities might be caused by the fact that the displacement rate of Manila could be modeled by the motion of neither the Sundaland nor the Eurasia plate. Then, we looked at velocities from the GNSS PIMO receiver which is located nearly 10 km northeast from the DORIS station and also belongs to the same orogen (dashed delimited area in Fig. 15). As depicted by Fig. 15, the horizontal velocity of PIMO (from 1999 doy 072 to 2009 doy 187) as extracted from ITRF2008 (Altamimi *et al.* 2011) is very similar to the one we obtained from DORIS (from 1993 doy 045 to 2014 doy 362). Moreover, these IDS and IGS horizontal vectors are consistent with the LAOA (GPS) residual vector with respect to Sundaland in Rangin *et al.* (1999) which concluded that there existed a counterclockwise rotation of the Luzon microblock with respect to the Sundaland plate. Even if we cannot deduce the Luzon motion from only one DORIS site, we can assert that the displacement of Manila has to be distinguished from the Sundaland and Philippine Sea plate motions.

4.2.4 Santiago (Chile)

Due to the San Juan Earthquake (M 5.7) in 2003 May 27, in Santiago (Chile), the new DORIS cumulative solution gives two velocity vectors: one for time period before (denoted by E1 on Fig. 16) and one after (denoted by E2 on Fig. 16) the Earthquake. However, these two IDS 09 horizontal velocities are very different in amplitude and direction from the predictions of both GEODVEL and NNR-MORVEL56. The superimposition of the velocities from the SANT (1997.0–2009.5) IGS station (see Fig. 16), located at nearly 73 m from DORIS stations SAOB and SANB (themselves 29 km northeast from the SANA DORIS station) shows that DORIS and GPS estimates have similar directions and that the magnitude of the DORIS E1 vector is smaller (18.8 mm yr^{-1} versus 27.1 mm yr^{-1}). The same observation follows from the estimations from the VLBI station with domes number 41705S006 (1992.0–1997.0) located at 206 m from the SANB DORIS station. Note that if we do not introduce the discontinuity due the San Juan Earthquake, as it was done in ITRF2008, then we get a unique DORIS velocity vector with magnitude of 24.4 mm yr^{-1}, a value which is comparable to the IGS and IVS estimations. Therefore, discrepancies between DORIS/GPS/VLBI and tectonic models reinforces the validity of the orogen hypothesized for the area by Bird (2003).

5 EVALUATION OF THE DORIS VERTICAL VELOCITIES

To assess the quality of the IDS 09 vertical velocities, we compared it to the latest GNSS cumulative solution (designated by ULR6) from La Rochelle University. That GNSS solutions was selected for several reasons: (i) it is based on a different geodetic space technique, (ii) the time span of ULR6 (1995.0–2014.0) is consistent with the IDS 09 one, (iii) more than 45 percent of the DORIS sites are co-located with GNSS sites included in ULR6 and

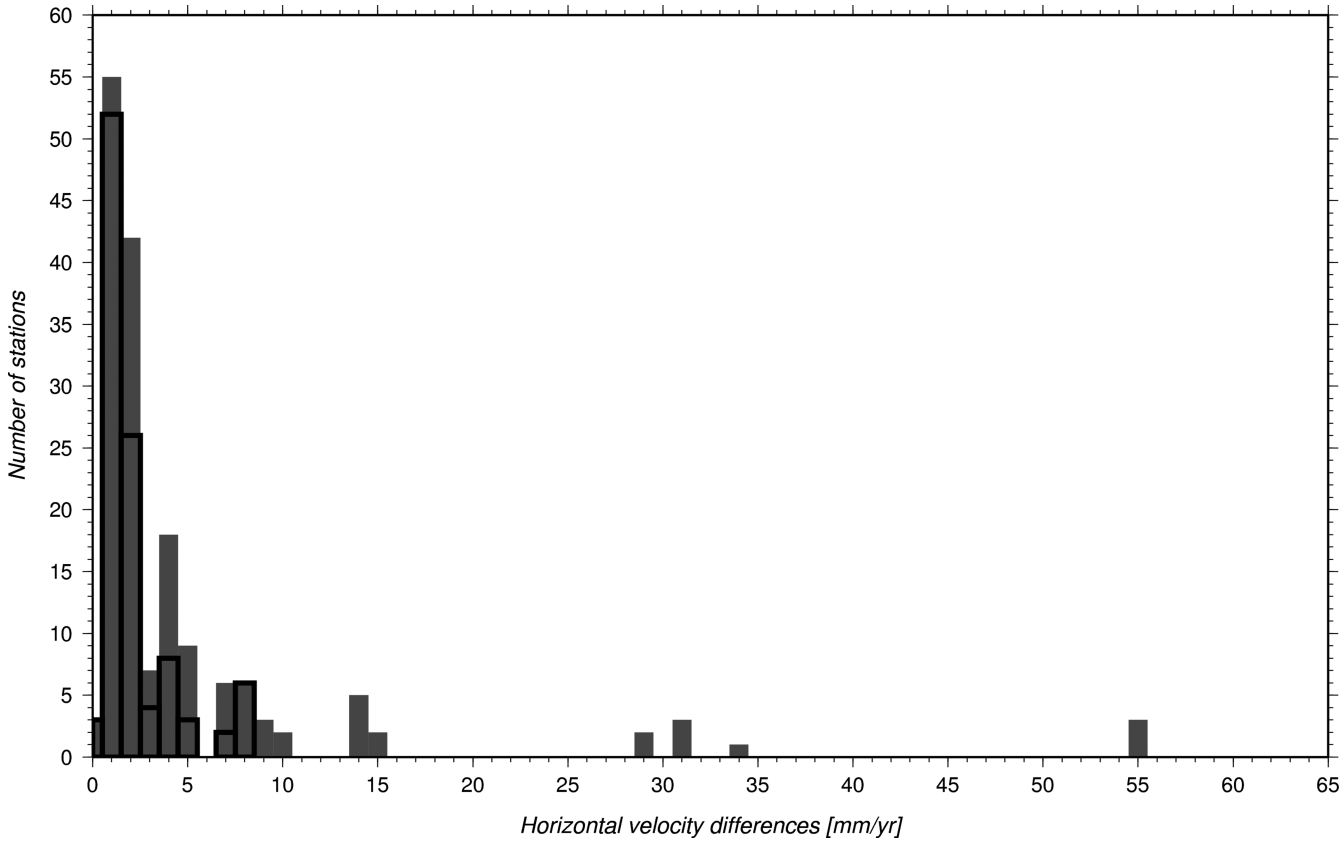

Figure 10. Histogram of the magnitude of the horizontal velocity differences between IDS 09 and GEODVEL. Black outlines indicate differences for the sites in the plate interiors.

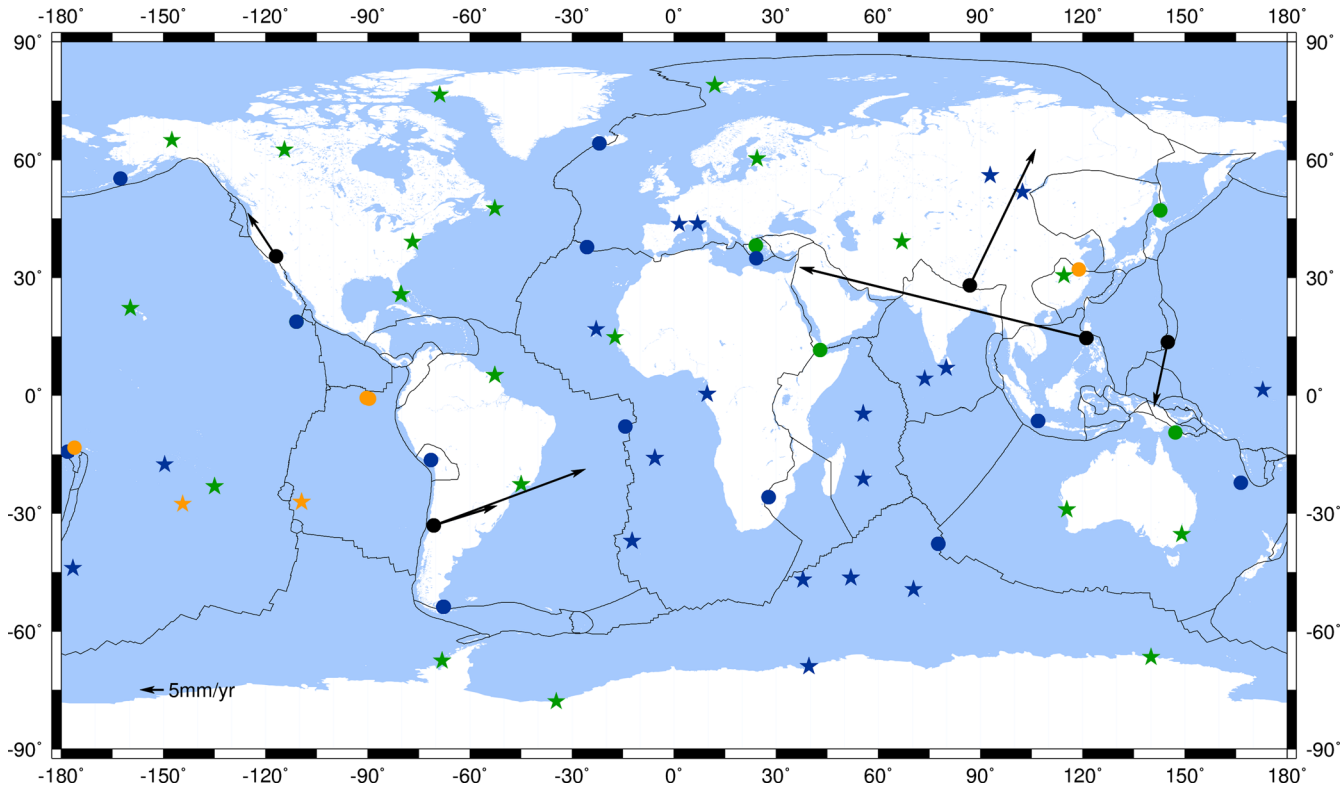

Figure 11. Horizontal velocity differences between IDS 09 and NNR-MORVEL56. Legend as in Fig. 9 excepted that grey lines indicate plate boundaries from the NNR-MORVEL56 model.

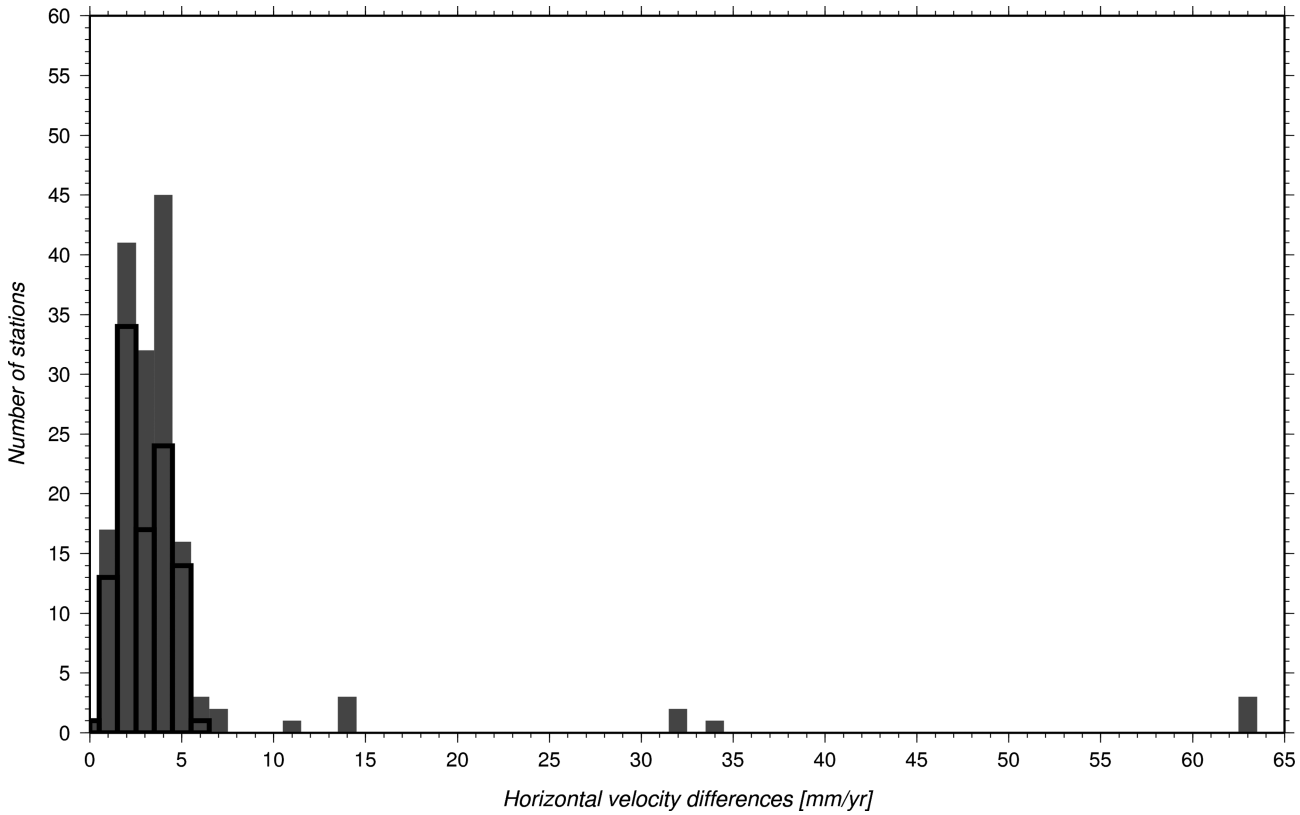

Figure 12. Histogram of the magnitude of the horizontal velocity differences between IDS 09 and NNR-MORVEL56. Black outlines indicate differences for the sites in the plate interiors.

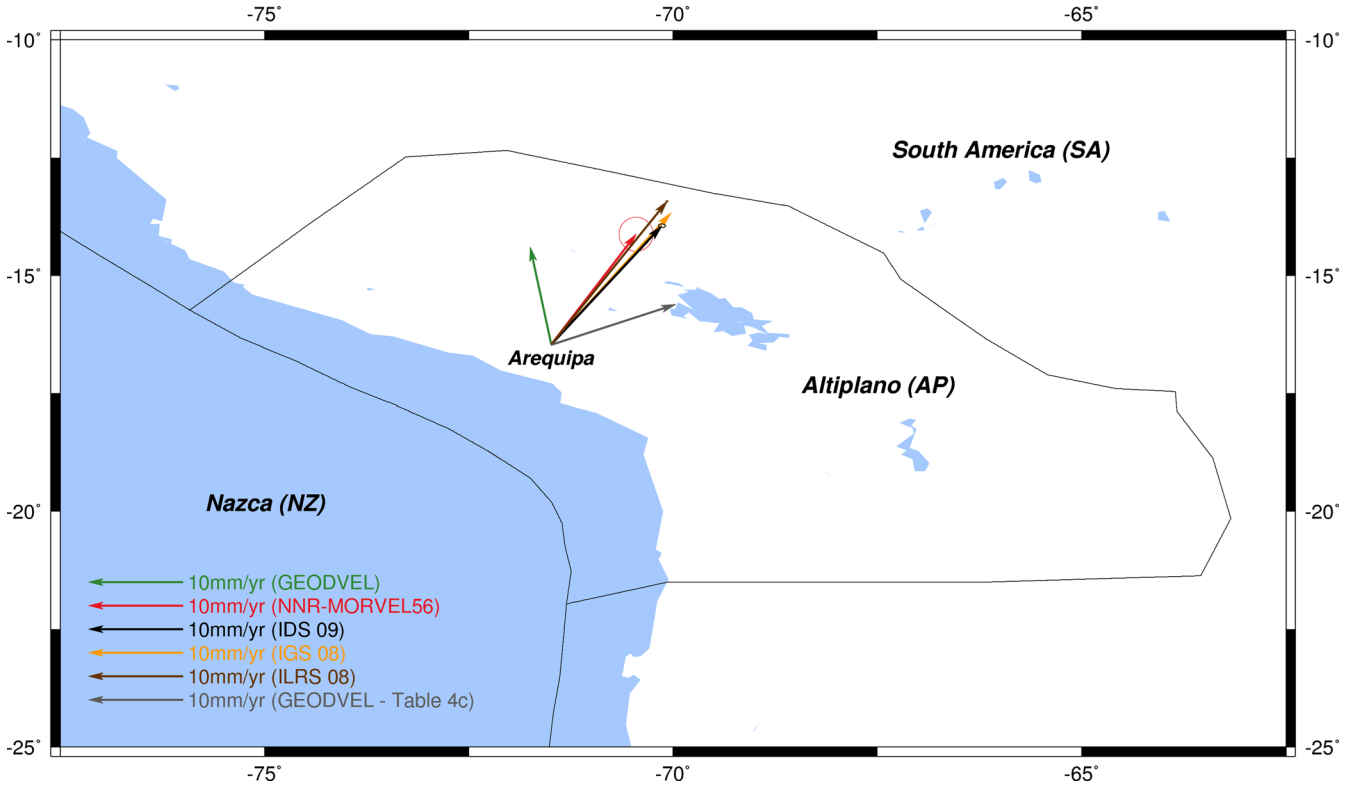

Figure 13. Horizontal velocities at Arequipa from IDS 09, GEODVEL, NNR-MORVEL56 and IGS and ILRS stations as extracted from ITRF2008. Grey lines indicate plate boundaries used by the NNR-MORVEL56 model.

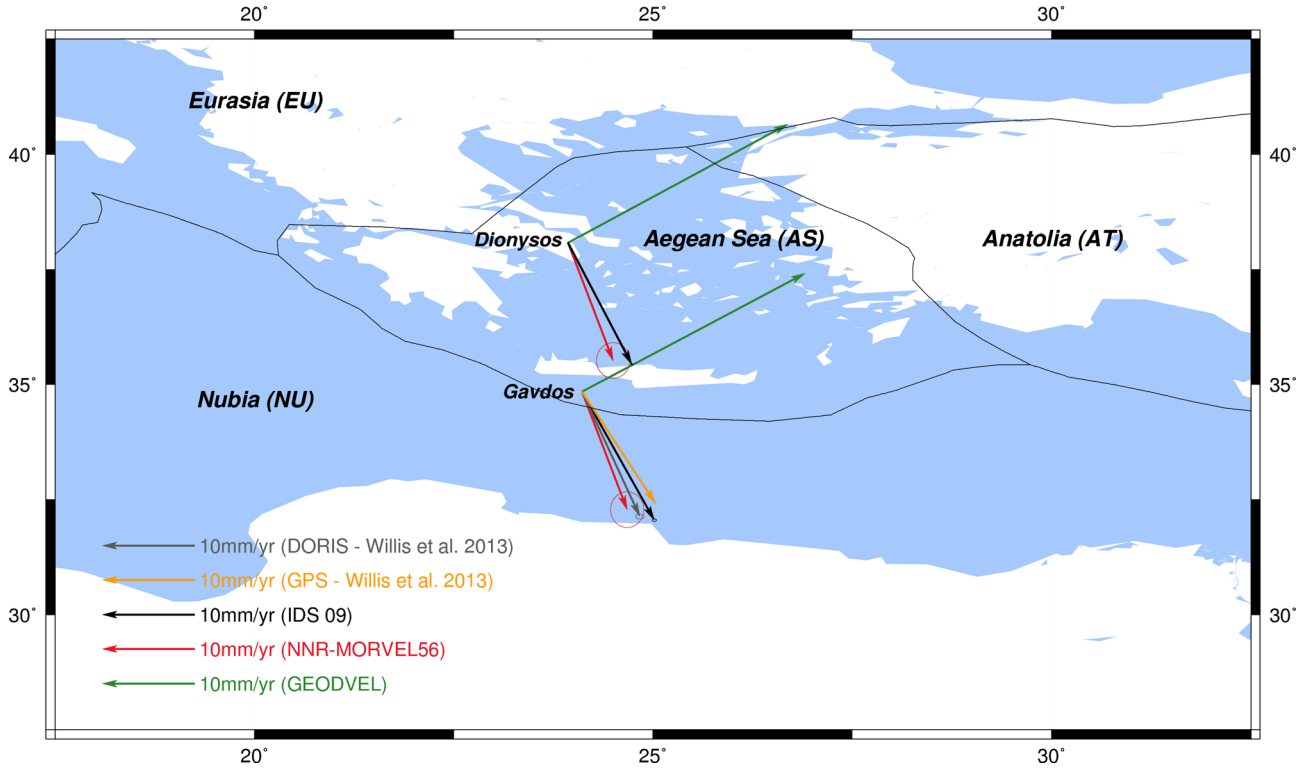

Figure 14. Horizontal velocities at Gavdos and Dionysos from GEODVEL, NNR-MORVEL56 and IDS 09.

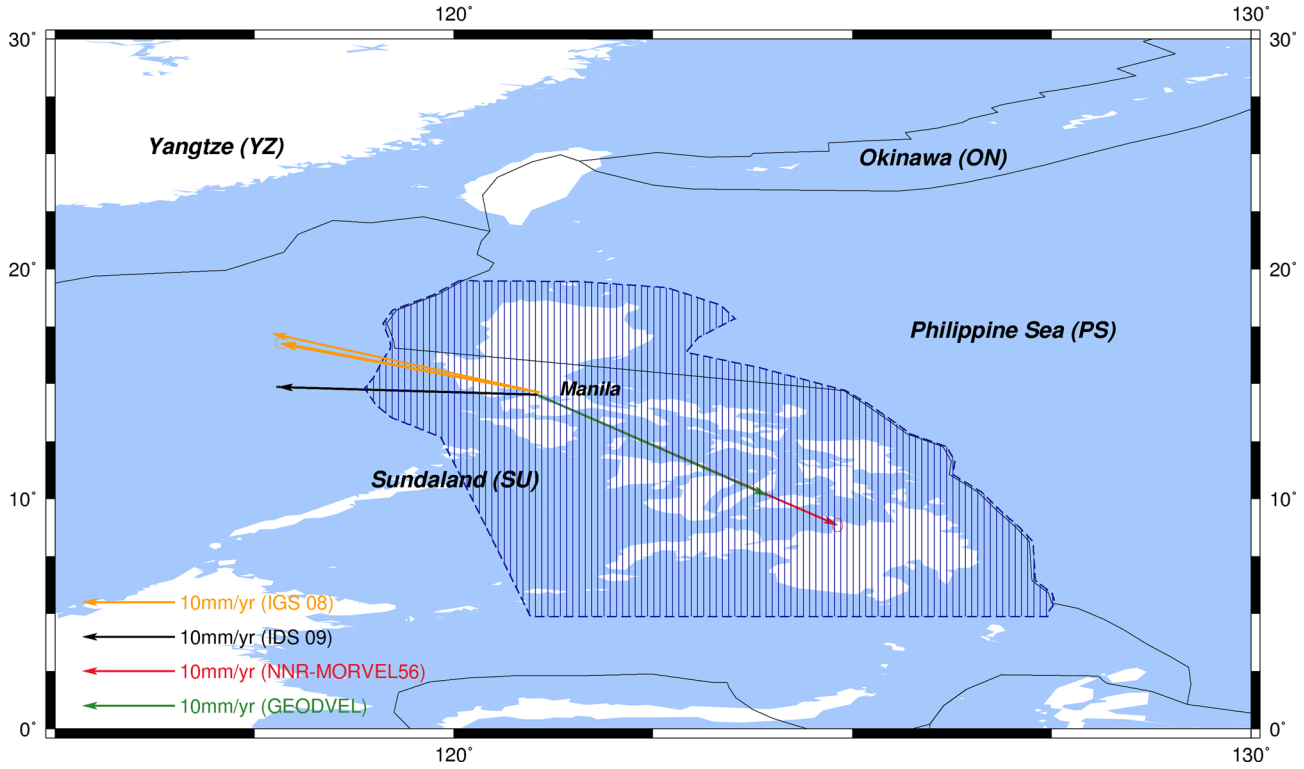

Figure 15. Horizontal velocities at Manila from GEODVEL, NNR-MORVEL56, IGb08 and IDS 09. Dashed zone corresponds to the Philippines orogen from Bird (2003).

(iv) La Rochelle University actively contributed to the IGS combined solution to ITRF2014. Nearly half of the DORIS sites are part of the ULR6 solution because tide gauge co-locations are part of the DORIS tracking network specifications and the ULR solutions are motivated by the estimations of vertical land motion in tide gauges. DORIS tide gauges co-locations can be seen as a consequence of the primary mission of the DORIS technique which consists in precise orbit estimations in support of altimetric missions. The estimation

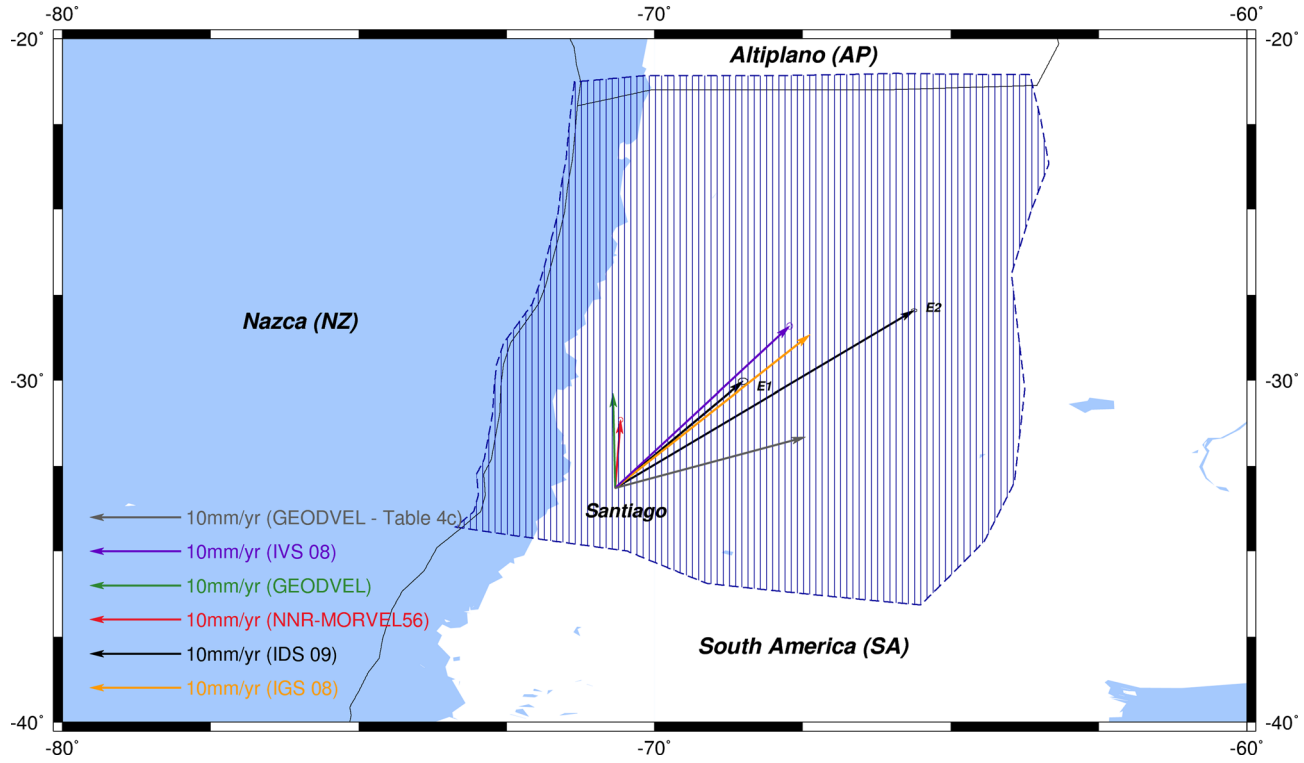

Figure 16. Horizontal velocities at Santiago from GEODVEL, NNR-MORVEL56, IGb08 and IDS 09. Dashed zone corresponds to orogen area from Bird (2003). E1 (respectively E2) designates the IDS 09 velocity vector before (respectively after) the San Juan Earthquake (2003 May 27—M 5.7).

of vertical land motion at tide gauge sites aims at deducing from tide gauge records geocentric sea level observations.

The last ULR GPS solution (ULR6) comprises 749 tracking stations with data covering the period 1995.0–2014.0. The GPS data processing includes the most up-to-date models and corrections compliant with the second IGS reprocessing campaign specifications. The station mean coordinates and velocities, aligned to the ITRF2008, were estimated following the same procedure described in Santamaría-Gómez *et al.* (2012).

5.1 IDS 09 versus ULR6

The comparison of vertical velocities at DORIS sites between IDS 09 and ULR6 cumulative solutions started by the determination of the GNSS stations in the neighbour of DORIS antennas. To do so, we first identified ULR6 stations sharing with DORIS stations the same five characters of its IERS DOMES number. Second, we deleted the ULR6 stations with vertical velocity uncertainties larger than 1 mm yr^{-1} and we selected couples of DORIS and GNSS stations with compatible data time span. Finally, for sites with several couples, we only kept couples corresponding to shorter tie vector lengths. Then, we get 34 couples of DORIS-GNSS stations at 31 over the 71 DORIS sites. Differences between IDS 09 and ULR6 estimations of the vertical motion at the 31 common sites are shown in Fig. 17. Note that 10 (white circles on Fig. 17) over the 34 couples have compatible vertical velocities, that is, velocities with differences smaller than the sum of the DORIS and GNSS formal errors. The rms of the vertical differences is 1.43 mm yr^{-1} and the correlation coefficient is 0.83.

From the histogram of the differences (see Fig. 18), we can see that at more than 60 percent of the sites (i.e. 21 sites) the differences are lower than 1 mm yr^{-1}. Similarly to the comparison of the horizontal velocities (see Section 4.2), we observe that the highest differences (orange, red and black dots on Fig. 17) between IDS 09 and ULR6 occur at plate boundaries or in seismic active zones (e.g. Galapagos, Goldstone, Guam, Noumea, Reykjavik and Rio-Grande). Differences in seismic active zones are the result of different observation time periods and/or discontinuities definition while cumulating the time-series to estimate the site velocities. Nevertheless, from Fig. 17, we also see that some of the biggest differences (black dots) are located in plate interiors: Mahé (MAHB, Seychelles), Miami (MIAB, USA), Rikitea (RIMB, Polynesia—France) and Thule (THUB, Greenland). For most of these sites (Guam, Miami and Rikitea), the differences may be explained by the short overlap between the DORIS and GNSS observation time span or the relative short time span for the DORIS sites. Moreover, as these sites are located between 30°S and 30°N and in coastal zones, the discrepancies may reflect some differences in the modeling of the troposphere influence. As displayed by Fig. 19, the differences between the IDS 09 and ULR6 vertical velocities do not seem to depend on the distance between the DORIS and the GNSS stations. For example, in Miami, even if the DORIS (MIAB) and GNSS (MIA3) stations are at a distance of around 295 m, the vertical velocity difference is 2.01 mm yr^{-1}. Note that the ULR6 estimation is similar to the JPL (http://sideshow.jpl.nasa.gov/) vertical velocities of the AOML (-0.34 ± 0.84 mm yr^{-1}, 230 m from MIAB) and MIA3 (-0.81 ± 0.50 mm yr^{-1}) GPS stations. Looking at the sitelog webpage of the DORIS station (http://ids-doris.org/network/sitelogs/), we note that the DORIS antenna is located on an upper terrace of a three-storey building. We also found that the AOML (respectively MIA3) antenna was located on top of a metal mat on top of a higher building (respectively a large pylon and not in IGS standards). Therefore, we cannot exclude that the vertical

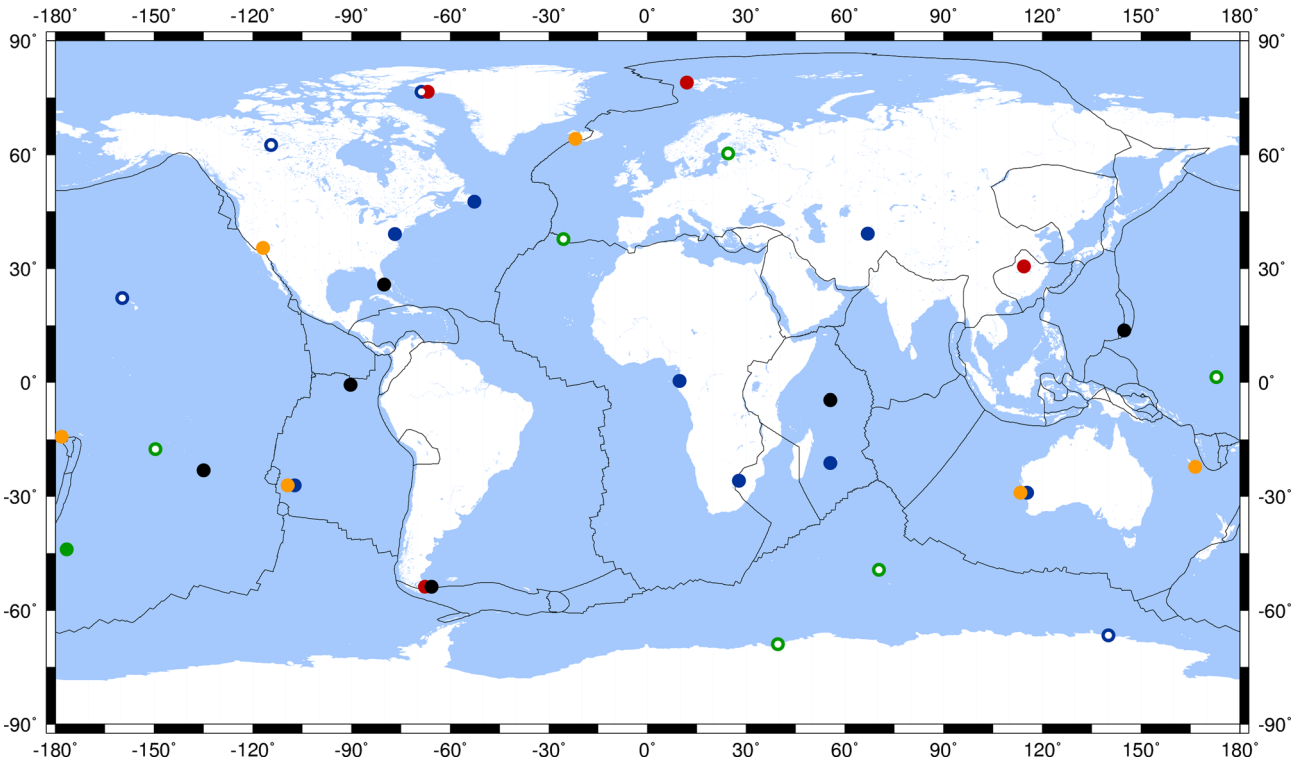

Figure 17. Vertical velocity differences between IDS 09 and ULR6. Green: less than 0.5 mm yr^{-1}. Blue: between 0.5 and 1.0 mm yr^{-1}. Orange: between 1.0 and 1.5 mm yr^{-1}. Red: between 1.5 and 2.0 mm yr^{-1}. Black: larger than 2 mm yr^{-1}. White dishes indicate stations for which the velocity difference is smaller than the sum of the IDS and ULR formal errors.

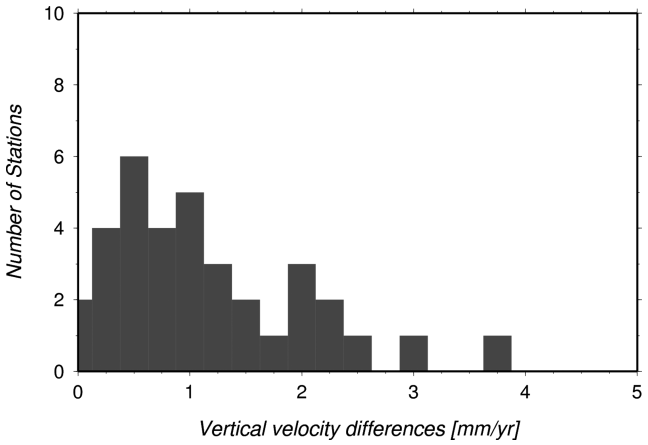

Figure 18. Histogram of the magnitude of the vertical velocity differences between IDS 09 and ULR6 cumulative solutions at the 31 sites of Fig. 17.

velocities from the DORIS and GNSS stations may not only reflect the geodetical process and so the vertical differences may be impacted by the type of support of the antenna. In the case of Mahé, the large velocity discrepancy (2.96 mm yr^{-1}), we cannot exclude that the distance (nearly 5.7 km) between the DORIS (MAHB) and GNSS (SEY1) stations is most probably part of the explanation. Moreover, as Mahé is a tropical island, the difference may also be related to differences in the troposphere modelization. Furthermore, note that the difference in Mahé was higher when comparing the DORIS and GPS ITRF2008 solutions. In Rikitea, the short distance (15 m) between these two stations cannot explain the velocity difference between the DORIS (RIKB/RILB/RIMB) and the GNSS (GAMB) estimations. The difference may also reflect differences in the troposphere modelization at that tropical island.

5.2 Thule (Greenland)

According to ICE-6G (Peltier *et al.* 2015), almost no significant GIA motion (amplitude of 0.1 ± 2 mm yr^{-1}) affects Thule (northwest coast of Greenland) so, GIA cannot explain the vertical uplift. Therefore, the vertical motion of Thule must be the consequence of recent phenomena. Monitoring the vertical motion of Thule is important with respect to sea level rise as well as to better evaluate the impact of the melting from polar ice sheets on the drifting of the Earth's pole as revealed by Chen *et al.* (2013). As displayed by Fig. 20 which represents time-series of the vertical component (expressed in ITRF2008) of the GPS (THU3—daily estimates—blue) and DORIS (THUB—weekly estimates—red) stations in Thule over the time span 2003.0–2015.0, we see similar pattern from the GPS and DORIS stations which are separated by around 61 m. However, the annual fluctuations are much larger with the GPS. In order to explain the origin of the uplift in Thule, we looked at the GRACE products as that gravimetric space mission revealed to be a powerful tool to monitor regional mass changes (Wahr *et al.* 1998).

Postglacial rebound at Thule is believed to be small, for example, vertical motion due to solid Earth's viscous response to unloading of the former ice sheets as predicted by ICE-6G is less than 1 mm yr^{-1}. Then, the decrease of the equivalent water height observed by GRACE can be interpreted as vertical uplift (response of an elastic Earth to mass loss). The similarity between the DORIS/GNSS and GRACE vertical coordinate time-series indicates that geometric and gravimetric techniques observe the same geophysical phenomenon. Moreover, it implies that the mass loss observed by GRACE is at

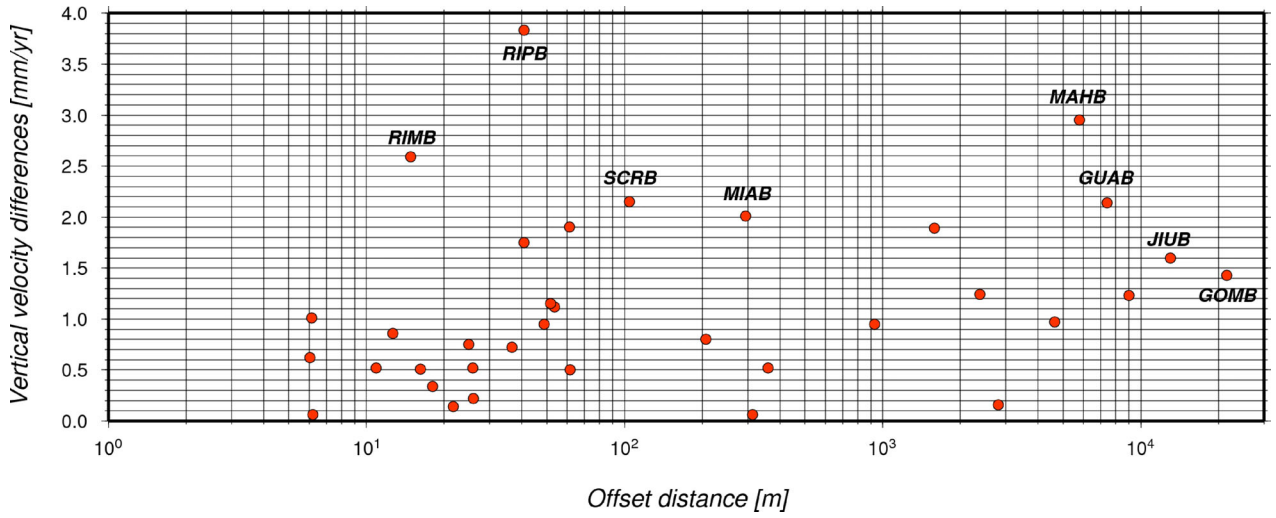

Figure 19. Vertical velocity differences as a function of the distance between the DORIS and GNSS stations.

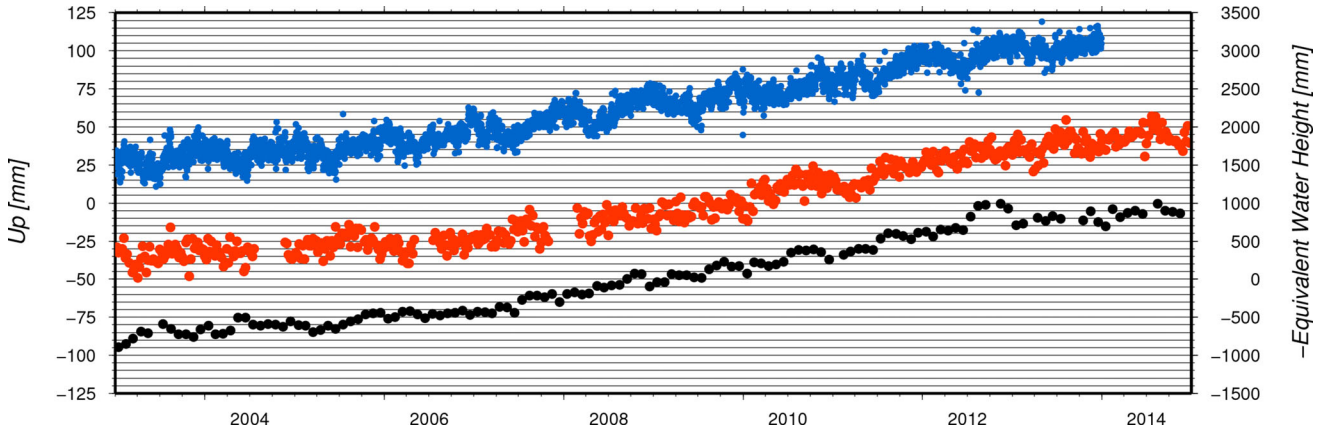

Figure 20. Time-series of the vertical component at long-term DORIS (THUB—red) and GNSS (THU3—blue) stations in Thule. Black dots correspond to minus the water height variations from monthly GRACE gravity fields. Each dot represents a daily solution for GNSS, a weekly solution for DORIS and a monthly solution for GRACE. The GNSS curve was shifted by +60 mm for better viewing. Vertical green lines correspond to 2006:196 and 2013:062.

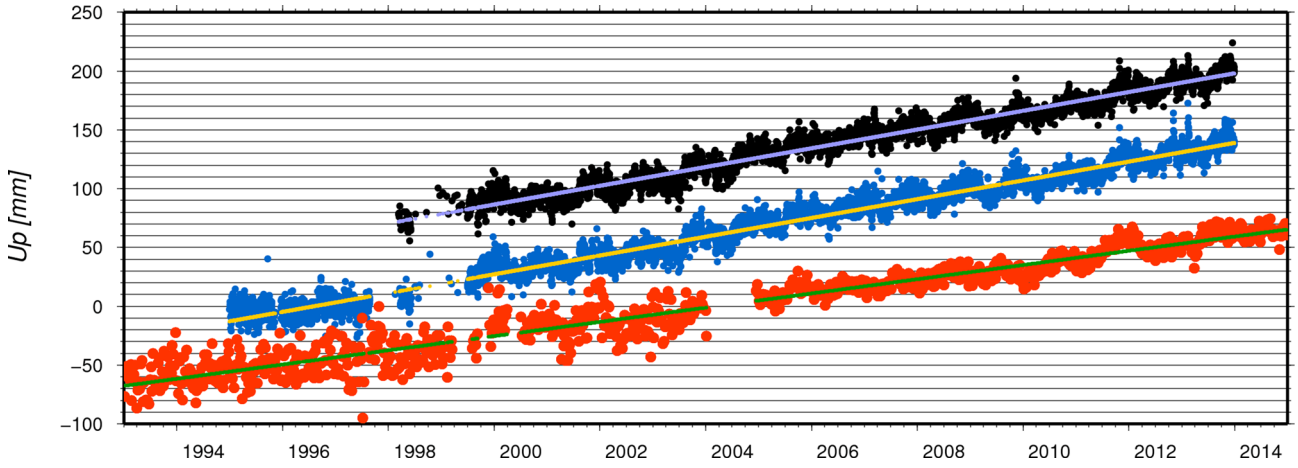

Figure 21. Time-series of the vertical component at long-term DORIS (SPIA, SPIB, SPJB—red) and GNSS (NYAL—blue; NYA1—black) stations in Ny-Ålesund. Each dot represents a daily solution for GNSS and a weekly solution for DORIS. NYAL and NYA1 curves were shifted by, respectively, +70 and +140 mm for better viewing.

the origin of the uplift observed by DORIS and GPS. Looking at the time evolution of the up component of the DORIS station, we identified an uplift acceleration in around 2006:096 (year:day of year) followed by a deceleration in 2013:062. Khan *et al.* (2010) explained that uplift increase by an accelerated mass loss dominated by outlet glaciers located along the coast. The deceleration may indicate that glaciers in that region have been stabilized. The introduction of these discontinuities gives three vertical velocities: 3.23 ± 0.34 mm

yr^{-1} before 2006:196, 9.43 ± 0.15 mm yr^{-1} between 2006:196 and 2013:062 and 3.74 ± 1.13 mm yr^{-1} after 2013:062. Similar uplift rates were obtained by linear regression of the GRACE equivalent water heights with, respectively, 3.45 mm yr^{-1} before 2006:196 and 9.95 mm yr^{-1} between 2006:196 and 2013:2013:062. That segmentation of the DORIS cumulative solution also explains the difference we observe on Fig. 17 as no discontinuity was introduced in the ULR6 cumulative solution while estimating vertical motions of the stations THU2 (6.83 ± 0.68 mm yr^{-1}) between 1998 and 2014 and THU3 (6.62 ± 0.74 mm yr^{-1}) between 2002 and 2014. Note that if no discontinuity is introduced in the computation of the IDS cumulative solution, then the vertical velocity of THUB (6.87 ± 0.07 mm yr^{-1}) would be similar to the GNSS estimations.

5.3 Ny-Ålesund (Svalbard—Norway)

The site of Ny-Ålesund is located on the shore of the Kings Fjord (Konkgsfjord) on the northwest coast of Spitsbergen, the main island of the Svalbard archipelago. According to Hagen *et al.* (2003), nearly 60 percent (i.e. about 36 600 km^2) of the land of the Svalbard archipelago is covered by glaciers and ice caps. Furthermore, several glaciers such as the Kongsbreen/Kronebreen (710 km^2), Kongsvegen (154 km^2), Brøggerbreen (Midtre/Vestre—17 km^2) and Lovénbreen (Austre/Midtre/Vestre—15 km^2) are at a maximum distance of 15–20 km from Ny-Ålesund. Thus, the geographic location of Ny-Ålesund makes valuable that site in the study of global change phenomena on ice melting and sea level. Ny-Ålesund is also of special interest as it is part of the geodetic station network of the Global Geodetic Observing System (Plag & Pearlman 2009). The geodetic infrastructure includes, in addition to the DORIS station, a VLBI (Very Long Baseline Interferometry) antenna, several GNSS (Global Navigation Satellite System) receivers, a tide gauge and a superconducting gravimeter. Thus, as all the sites with more than three of the geodetic techniques, Ny-Ålesund plays a key role in the determination and maintenance of the ITRF by connecting the different techniques. As deduced from the DORIS stations SPIA, SPIB and SPIJB, the vertical velocity is of 6.13 ± 0.07 mm yr^{-1}. Results from ULR6 at NYAL station, located 1.6 km northwest from the DORIS stations, gives a velocity of 7.97 ± 0.48 mm yr^{-1}. Similar uplift is obtained from the GNSS NYA1 station (8.02 ± 0.50 mm yr^{-1}) located at 8 m from NYAL. These GPS uplift rates are close to the estimates by Mémin *et al.* (2014) for NYA1 and NYAL between 2000 and 2013. Then, the uplift rates from DORIS and GNSS are more than two times larger than that predicted GIA models (2.38 mm yr^{-1} from ICE-6G). Therefore, the vertical motion may also include more recent phenomena such as the retreat of the Lovénbreen glacier in the vicinity of Ny-Ålesund. From Kierulf *et al.* (2009b), in Ny-Ålesund, uplift due to current ice loss is estimated to be 3.2 mm yr^{-1} for the period between 1993 and 2008. According to Mémin *et al.* (2014), depending on the total volume of ice loss of glaciers located between 2 and 110 km from Ny-Ålesund, the rate of vertical displacement induced by current ice loss varies from 1.88 to 3.52 mm yr^{-1}. Then, GIA and current ice loss lead to an uplift of 4.26 to 5.90 mm yr^{-1} which is compatible with the DORIS estimation. Nevertheless, it leaves an excess uplift of around 2 mm yr^{-1} according to GNSS. Furthermore, as pointed out by King & Watson (2014), the comparison of the DORIS and GNSS vertical velocities with vertical motion over much longer timescales may also be biased by non-linear rapid motion of the rotation pole since 2005. Note that earlier studies have pointed out the inconsistency between the different observing techniques (GNSS and VLBI) in Ny-Ålesund (Sato *et al.* 2006; Kierulf *et al.* 2009a). As no monument instability has been identified and since the ULR velocities are similar to other GPS solutions, and since the GPS and DORIS stations are only separated by 1.6 km, the inconsistency may be due to non-optimum estimation of the solar radiation pressure which induces systematic errors in the heights of high latitude stations. Nonetheless, based on the coordinate time-series from the DORIS, GPS and VLBI stations as computed by, respectively, the IDS, IGS and IVS CCs from their contributions to ITRF2014, Tornatore *et al.* (2016) get compatible vertical velocities with 6.1, 6.8 and 6.3 mm yr^{-1}, respectively. Even if the DORIS uplift rate from Tornatore *et al.* (2016) is equal to the one we obtained whereas they modelized non-linear and periodic terms while estimating the linear trend, we can assume that their more precise estimations coupled with the use of combined solutions for the two other geodetic techniques can explain why they get such more similar results between the techniques.

6 CONCLUSIONS

In this study, we evaluated both the horizontal and vertical velocities from the cumulative position and velocity solution associated with the DORIS contribution to ITRF2014 (Moreaux *et al.* 2016). Prior to the evaluation, we describe how the mean position and velocity of 222 stations (as expressed in ITRF2008) were obtained from the 1140 weekly IDS combined solution files over the time span 1993.0–2015.0 (see Section 2). This total number of stations includes the 62 discontinuities of the Table 1 identified from the coordinate time-series of the 71 DORIS sites. Analysis of the velocity showed that 191 (respectively 201) of the horizontal (respectively vertical) formal errors are smaller than 1 mm yr^{-1}. The four sites with higher formal errors are part of the seven DORIS sites with the smallest number of weeks of observations.

As a preliminary step of the evaluation of the horizontal velocities with respect to the global plate models GEODVEL (Argus *et al.* 2010) and NNR-MORVEL56 (Argus *et al.* 2011), from the ICE-6G model (Peltier *et al.* 2015), the GIA effect was subtracted to the DORIS estimates. Due to the inclination of the DORIS satellite orbits, the DORIS horizontal velocities present larger differences in the east direction compared to the plate models (*cf.* Section 4). Nevertheless, for more than 55 percent of the DORIS sites, the rms of the differences is smaller than 3 mm yr^{-1}. As expected, most of the sites with the largest discrepancies are located in seismic regions and close to the plate boundaries. A detailed analysis and comparison was performed for the five DORIS sites (Arequipa, Peru; Dionysos, Gavdos, Greece; Manila, Philippines; and Santiago, Chile) with the largest discrepancies with respect to the two global plate models. In Arequipa and Santiago, comparisons with GNSS and/or laser velocities as extracted from ITRF2008 showed agreements with the DORIS estimates. Investigations on Dionysos and Gavdos sites (Greece) reveal that the differences with the GEODVEL predictions are implied by the lack of a local small plate: the SW Aegean/Pelopponnisos plate. Moreover, the DORIS horizontal velocities agree with the southwestward motion of the Aegean region with respect to Eurasia at 30 mm yr^{-1}. We also show that in Manila the differences are the consequence of a local microplate and that the DORIS horizontal velocity supports a counterclockwise rotation of the Luzon microblock with respect to the Sundaland plate.

The evaluation of the DORIS vertical velocities consisted in comparisons with the ULR6 GPS solution from La Rochelle

University at 31 of the 71 DORIS sites. The two solutions show a good agreement with a correlation coefficient of 0.83 and an rms of the differences of 1.43 mm yr^{-1}. Furthermore, for 60 percent of the DORIS-GPS co-located sites, the difference of the vertical motions is below 1 mm yr^{-1}. Similarly to the horizontal velocities, we observe that the largest differences between the DORIS and GPS vertical motion estimations are located at plate boundaries and in seismic active zones. Moreover, the vertical motion differences do not seem to be correlated with the distance between the DORIS and GPS stations. While comparing the vertical DORIS velocities to the ICE-6G model, we found a correlation coefficient of 0.45 for all the sites and of 0.62 for the sites in plate interiors. The differences with ICE-6G may result from the fact that the DORIS vertical velocities includes more recent phenomena such as current ice loss. Investigations on the origin of the disagreement between the DORIS and ULR6 uplift rates in Thule (Greenland) show that it is due to the introduction in the DORIS solution of two velocity discontinuities in 2006:196 and in 2013:062. The DORIS observations indicate a notable uplift acceleration mid-2006 (from 3.23 ± 0.34 to 9.43 ± 0.15 mm yr^{-1}) and a deceleration early 2012 (from 9.43 ± 0.15 to 3.74 ± 1.13 mm yr^{-1}). While the first event is explained by an accelerated mass loss is from outlet glaciers located along the coast as suggested by Khan *et al.* (2010), the second event is still unexplained. Meanwhile, as the newest uplift rate is similar to the vertical velocity before mid-2006, and as the phenomena is also observable on the GRACE measurements (see Fig. 20), we can assume that it is due to a deceleration of mass loss and may indicate that the outlet glaciers have reached an equilibrium point. However, that assumption will have to face more recent DORIS, GPS and GRACE observations as well as glaciological measurements on the outlet glaciers of Thule. In the case of Ny-Ålesund, further analysis show that the DORIS uplift rate is compatible with the sum of GIA and current ice loss motions while GPS observations induce an excess uplift of around 2 mm yr^{-1}.

Finally, this study showed the validity of the DORIS horizontal and vertical velocities and emphasizes the use of the DORIS observations in the monitoring of geophysical process like Earthquakes and ice melting. DORIS may also be of good help in areas with sparse geodetic networks such as Africa or Antarctica. Moreover, all these DORIS products will benefit in terms of both availability and accuracy from the future satellites carrying the new generation of DORIS receivers coupled with a next generation of DORIS ground beacons combined and a consolidated model of ground antennas.

ACKNOWLEDGEMENTS

Part of this work was supported by Centre National d'Etudes Spatiales (CNES) and is based on observations from the DORIS satellites. DFA's part of this research was performed at Jet Propulsion Laboratory under contract with NASA. All the DORIS data used in this study are freely available and downloadable from the IDS data centres: CDDIS (ftp://cddis.gsfc.nasa.gov/doris/products/) and IGN (ftp://doris.ensg.ign.fr/pub/doris/). The GPS solution from University of La Rochelle is available at http://www.sonel.org. The University of La Rochelle computing infrastructure was partly funded by the European Union (contract 31031-2008, European Regional Development Fund). The SONEL GPS@TG data assembly centre is supported by INSU/CNRS. Figures were produced with the Generic Mapping Tool software (Wessel & Smith 1991).

REFERENCES

Altamimi, Z., Boucher, C. & Sillard, P., 2002. New trends for the realization of the international terrestrial reference system, *Adv. Space Res.,* **30**(2), 175–184.

Altamimi, Z., Collilieux, X. & Métivier, L., 2011. ITRF2008: an improved solution of the international reference frame, *J. Geod.,* **85,** 457–473.

Altamimi, Z., Rebischung, P., Métivier, L. & Collilieux, X., 2016. ITRF2014: A new release of the International Terrestrial Reference Frame modeling non-linear station motions, *J. geophys. Res.,* doi:10.1002/2016JB013098.

Argus, D.F., Gordon, R.G., Heflin, M.B., Ma, C., Eanes, R.J., Willis, P., Peltier, W.R. & Owen, S.E., 2010. The angular velocities of the plates and the velocity of Earth's Center from Space Geodesy, *Geophys. J. Int.,* **180**(3), 913–960.

Argus, D.F., Gordon, R.G. & DeMets, C., 2011. Geologicallly current motion of 56 plates relative to the no-net-rotation reference frame, *Geochem. Geophys. Geosyst.,* **12,** Q11001, doi:10.1029/2011GC003751.

Argus, D. F, Peltier, W.R., Drummond, R. & Moore, A.W., 2014. The Antarctica component of postglacial rebound model ICE-6G_C (VM5a) based on GPS positioning, exposure age dating of ice thicknesses, and relative sea level histories, *Geophys. J. Int.,* **198**(1), 537–563.

Bettinelli, P., Avouac, J.P., Flouzat, M., Jouanne, F., Bollinger, L., Willis, P. & Chitrakar, G.R., 2006. Plate motion of india and interseismic strain in the Nepal Himalaya from GPS and DORIS measurements, *J. Geod.,* **80**(8–11), 567–589.

Bird, P., 2003. An updated digital model of plate boundaries, *Geochem. Geophys. Geosyst.,* **4**(3), 1027, doi:10.1029/2001GC000252.

Capdeville, H., Štěpánek, P., Hecker, L. & Lemoine, J.-M., 2016. Update of the corrective model for Jason-1 DORIS data in relation to the South Atlantic Anomaly and a corrective model for SPOT-5, *Adv. Space Res.,* in press, doi:10.1016/j.asr.2016.02.009.

Chen, J.L., Wilson, C.R., Ries, J.C. & Tapley, B.D., 2013. Rapid ice melting drives Earth's pole to the east, *Geophys. Res. Lett.,* **40**(11), 2625–2630.

Crétaux, J.-F., Soudarin, L., Cazenave, A. & Bouillé, F., 1998. Present-day tectonic plate motions and crustal deformations from the DORIS space system, *J. Geophys. Res.,* **103**(B12), 30 167–30 181.

DeMets, C., Gordon, R.G. & Argus, D.F., 2010. Geologically current plate motions, *Geophys. J. Int.,* **181,** 1–80.

Farrell, W., 1972. Deformation of the Earth by surface loads, *Rev. Geophys.,* **10,** 761–797.

Gegout, P., Boehm, J. & Wijaya, D., 2010. Practical numerical computation of Love numbers & applications. Workshop of the COST Action ES0701, Vienna, 16–17 November 2010. Available at: http://ggosatm.hg.tuwien.ac.at/LOADING/COSTES0701/04_2010_COST_Vienna_Gegout.pdf, last accessed 1 August 2016.

Hagen, J.O., Kohler, J., Melvold, K. & Winther, J.G., 2003. Glacier atlas of Svalbard and Jan Mayen, *Polar Res.,* **22**(2), 145–159.

Khan, S.A., Wahr, J., Bevis, M., Velicogna, I. & Kendrick, E., 2010. Spread of ice mass loss into northwest Greenland observed by GRACE and GPS, *Geophys. Res. Lett.,* **37,** L06501, doi:10.1029/2010GL042460.

Kierulf, H.P., Pettersen, B., McMillan, D.S. & Willis, P., 2009a. The kinematics of Ny-Alesund from space geodetic data, *J. Geodyn.,* **48**(1), 37–46.

Kierulf, H.P., Plag, H.-P. & Kohler, J., 2009b. Surface deformation induced by present-day ice melting in Svalbard, *Geophys. J. Int.,* **179**(1), 1–13.

King, M.A. *et al.*, 2010. Improved constraints on models of glacial isostatic adjustment: a review of the contribution of ground-based geodetic observations, *Surv. Geophys.,* **31**(5), 465–507.

King, M.A. & Santamaría-Gómez, A., 2016. Ongoing deformation of Antarctica following the Great Earthquakes, *Geophys. Res. Lett.,* **43,** 1918–1927.

King, M.A. & Watson, C.S., 2014. Geodetic vertical velocities affected by recent rapid changes in polar motion, *Geophys. J. Int.,* **199**(2), 1161–1165.

Kreemer, C., Blewitt, G. & Klein, E.C., 2014. A geodetic plate motion and Global Strain Rate Model, *Geochem. Geophys. Geosyst.,* **15,** 3849–3889.

Lemoine, J.-M. & Capdeville, H., 2006. A corrective model for Jason-1 DORIS Doppler data in relation to the South Atlantic Anomaly, *J. Geod.,* **80**(8–11), 507–523.

McClusky, S. *et al.*, 2010. Global Positioning System constraints on plate kinematics and dynamics in the eastern Mediterranean and Caucasus, *J. geophys. Res.,* **105,** 5695–5719.

Mémin, A., Spada, G., Boy, J-.P., Rogister, Y. & Hinderer, J., 2014. Decadal geodetic variations in Ny-Ålesund (Svalbard): role of past and present ice-mass changes, *Geophys. J. Int.,* **198**(1), 285–297.

Moreaux, G., Lemoine, F.G., Capdeville, H., Kuzin, S., Otten, M., Štěpánek, P., Willis, P. & Ferrage, P., 2016. The International DORIS Service contribution to the 2014 realization of the International Terrestrial Reference Frame, *Adv. Space Res.,* in press, doi:10.1016/j.asr.2015.12.021.

Nocquet, J.-M., Willis, P. & Garcia, S., 2006. Plate kinematics of Nubia-Somalia using a combined DORIS and GPS solution, *J. Geod.,* **80**(8–11), 591–607.

Peltier, W.R., Argus, D.F. & Drummond, R., 2015. Space geodesy constrains ice-age terminal deglaciation: the global ICE-6G_C (VM5a) model, *J. geophys. Res.,* **120,** 450–487.

Plag, H.-P. & Pearlman, M., 2009. *Global Geodetic Observing System: Meeting the Requirements of a Global Society on a Changing Planet in 2020,* Springer.

Rangin, C., Le Pichon, X., Mazzotti, S., Pubellier, M., Chamot-Rooke, N., Aurelio, M., Walpserdorf, A. & Quebral, R., 1999. Plate convergence measued by GPS across the Sundaland/Philippine Sea Plate deformed boundary: the Philippines and eastern Indonesia, *Geophys. J. Int.,* **139**(2), 296–316.

Rudenko, S. *et al.*, 2014. Influence of time variable geopotential models on precise orbits of altimetry satellites, global and regional mean sea level trends, *Adv. Space Res.,* **54**(1), 92–118.

Santamaría-Gómez, A., Gravelle, M., Collilieux, X., Guichard, M., Martin Miguez, B., Tiphaneau, P. & Wöppelmann, G., 2012. Mitigating the effects of vertical land motion in tide gauge records using a state-of-the-art GPS velocity field, *Glob. Planet. Change,* **98–99,** 6–17.

Saria, E., Calais, E., Altamimi, Z., Willis, P. & Farah, H., 2013. A new velocity field for Africa from combined GPS and DORIS space geodetic solutions: contribution to the definition of the African reference frame (AFREF), *J. geophys. Res.,* **118**(4), 1677–1697.

Sato, T., Okuno, J., Hinderer, J., MacMillan, D.S., Plag, H.-P., Francis, O., Falk, R. & Fukuda, Y., 2006. A geophysical interpretation of the secular displacement and gravity rates observed at Ny-Ålesund, Svalbard in the Arctic—effects of post-glacial rebound and present-day ice melting, *Geophys. J. Int.,* **165**(3), 729–743.

Soudarin, L. & Crétaux, J.-F., 2006. A model of present-day tectonic plate motions from 12 years of DORIS measurements, *J. Geod.,* **80**(8–11), 609–624.

Štěpánek, P., Dousa, J. & Filler, V., 2014. SPOT-5 DORIS oscillator instability due to South Atlantic Anomaly: mapping the effect and application of data corrective model, *Adv. Space Res.,* **52**(7), 1355–1365.

Tapley, B.D., Bettadpur, S., Watkins, M. & Reigber, C., 2004. The gravity recovery and climate experiment: mission overview and early results, *Geophys. Res. Lett.,* **31**(9), L09607, doi:10.1029/2004GL019920.

Tornatore, V., Kayıkçı, E.T. & Roggero, M., 2016. Comparison of ITRF2014 station coordinate input time series of DORIS, VLBI and GNSS, *Adv. Space Res.,* in press, doi:10.1016/j.asr.2016.07.016.

Tourain, C., Moreaux, G., Auriol, A. & Saunier, J., 2016. DORIS Starec ground antenna characterization and impact on positioning, *Adv. Space Res.,* in press, doi:10.1016/j.asr.2016.05.013.

Wahr, J., Molenaar, M. & Bryan, F., 1998. Time variability of the Earth's gravity field: hydrological and oceanic effects and their possible detection using GRACE, *J. geophys. Res.,* **103**(B12), 30 205–30 229.

Wessel, P. & Smith, W.H.F., 1991. Free software helps map and display data, *EOS, Trans. Am. geophys. Un.,* **72,** 441–446.

Willis, P., Ries, J.C., Zelensky, N.P., Soudarin, L., Fagard, H., Pavlis, E.C. & Lemoine, F.G., 2009. DPOD2005: an extension of ITRF2005 for precise orbit determination, *Adv. Space Res.,* **44**(5), 535–544.

Willis, P., Mertikas, S., Argus, D.F. & Bock, O., 2013. DORIS and GPS monitoring of the Gavdos calibration site in Crete, *Adv. Space Res.,* **51**(8), 1438–1447.

Willis, P. *et al.*, 2016a. DPOD2008, A DORIS-oriented Terrestrial Reference Frame for Precise Orbit Determination, *IAG Symposia Series,* **143,** 175–181.

Willis, P. *et al.*, 2016b. The International DORIS Service (IDS), Recent Developments in Preparation for ITRF2013, *IAG Symposia Series,* **143,** 631–639.

APPENDIX: GRACE EQUIVALENT WATER HEIGHT

GRACE is a joint mission between NASA (National Aeronautic and Space Administration) and DLR (German Space Agency), which was launched in 2002 March 2002 is still in orbit. GRACE is made of a pair of satellites, following each other on a polar orbit (inclination of 89°), at an altitude of approximately 500 km and at a distance of 220 km. The main instrument is the K-Band Ranging system, an electromagnetic link in the *K*/*Ka* band, which allows to measure the distance variations between the two satellites. The GRACE data allow to detect from the variations of Earth's gravity field the movements of mass at the Earth's surface, such as hydrological cycle, ice loss and Earthquakes. Thus, the GRACE results can be used to estimate crustal uplift, which can be compared with the DORIS and the GNSS data. Loading or unloading of the crust from changes in surface mass cause vertical crustal displacements with amplitudes dependent on the amplitude of the load and on the distance between the load and the observing point (Farrell 1972). Accelerated mass loss from nearby regions would thus cause accelerated vertical crustal uplift. We use monthly equivalent water height estimations generated and made publicly available (http://thegraceplotter.com) by the Groupe de Recherche de Géodésie Spatiale (GRGS). Pointwise estimations of equivalent water heights are obtained by interpolation of 1°-by-1° equivalent water heights grids. Grids were computed from equivalent water height spherical harmonic coefficients from degree 2 to 80. The equivalent water height coefficients were deduced from the gravity coefficients by mean of Love numbers (Gegout *et al.* 2010). Note that the C20 gravity coefficient was unchanged since CNES/GRGS solutions contain satellite laser ranging data (Lageos 1 and 2, Starlette, Stella up to degree 30).